João Ricardo Antunes Afonso

Licenciado em Ciências de Engenharia
de Micro e Nanotecnologias

Tuning the electronic properties of ZnO and $CuCrO_2$ though annealing for transparent electronic applications

Dissertação para obtenção do Grau de Mestre em
Engenharia de Micro e Nanotecnologias

Orientador: Dr. Elvira Maria Correia Fortunato, Prof. Catedrática, FCT-UNL
Co-orientador: Dr. Renaud Leturcq, Lead R&T Associate, LIST

Júri:

Presidente: Prof. Doutor Rodrigo Martins
Arguente: Prof. Doutor Jonas Deuermeier
Vogal: Prof. Doutora Elvira Fortunato

FACULDADE DE CIÊNCIAS E TECNOLOGIA
UNIVERSIDADE NOVA DE LISBOA

September 2017

Tuning the electronic properties of ZnO and $CuCrO_2$ though annealing for transparent electronic applications

Acknowledgements

It is with great satisfaction that I see the end of my university journey. It was not an easy journey, it had pleasure, laughs, parties but had also lots of difficulties and obstacles along the way, and I happy truly happy with the way things composed during the time and the way I improved as a person during my path to be a Master in Micro and Nanotechnology Engineer.

For this I would like to thank the Institution, Faculdade de Ciências e Tecnologias, specially Departamento de Ciencias dos Materiais and CENIMAT. I would like to thank all the teachers that crossed my path during this journey, mainly to my supervisor Elvira Fortunato, for all the help and for all the effort putting towards the evolution of this course and of the research in Portugal.

I would like to thank my receiving organization LIST, that permitted me to develop my work towards my thesis. It was a fantastic opportunity where I met fantastic person and that permitted me to evolve a lot and discover a completely new working method, the approach of a RTO. I would like to thank Damien Lenoble and Petru Popa, for all the help, support, supervision and teaching they gave me. Mostly Renaud Leturcq, my supervisor, gave me a fantastic help, in what I found to be a good approach, transmitting a lot of knowledge, helping me giving a direction to my work but giving me the freedom to take decisions, I think this was very important for my satisfaction during this work. All his constant support in harder times needs to be thanked. I would also like to thank the colleagues I found, Nohora, Serena, David, Sabrina, Sunil, Hameeda and Tai, and mainly to my friend Rishabh.

My parents that always supported me, from way before this journey supported in all the possible ways, giving me all the opportunities I could ask for and permitting always that I draw my way and took my personal decisions. To my little sister Beatriz for the relaxing moments.

To all my friends that I found in university, Pinela, Marco, Tiago, Coroa and Shiv, for all the supporting moments where we shared questions and doubts and studied together and for the enjoying moments, and to my friends from before, all my friends mainly, Eusebio, Henrique, Margarida, Guilherme, Bernardo, Bela and Bruno. To Laura, always supported me along this journey for all the moments.

ABSTRACT

Transparent microelectronics applications have been receiving a great amount of research because of the continuous demand for better products from the consumers due to their use in almost every product of the modern-day society. This work comes to explore two of the missing building blocks in completely transparent microelectronics, a capable transparent conductive oxide (TCO) that can substitute indium-tin-oxide (ITO) and a good transparent p-type TCO. The materials studied were ZnO and $CuCrO_2$ that were tuned for a wide range of carrier concentration though changes in deposition parameters and annealing steps. ZnO thin films have shown a wide range of carrier concentration from $8 * 10^{19}$ approaching $10^{18}\ cm^{-3}$ and even values above $10^{20}\ cm^{-3}$, in the case of Aluminium doped ZnO films. An important relationship was discovered during this work, a direct interplay of the mobility with the carrier concentration, $\mu \propto n$, that holds in the range between $10^{18} - 3 * 10^{19} cm^{-3}$. $CuCrO_2$ thin films have shown also a wide range of tunability in terms of carrier concentration from $2 * 10^{21}$ to $10^{17}\ cm^{-3}$, showing a progressive increase of optical transmittance from 37% to 60% with the decrease in carrier concentration, which makes them more suitable for transparent electronics applications. A P-N junction was proposed with these materials with a projected type-II band alignment and optimized carrier concentration of about $5 * 10^{18}\ cm^{-3}$ on both sides of the junction. The junction was patterned by etching and photolithography but unfortunately the carrier concentration was not the optimized one, that lead into a ohmic contact.

Keywords: ZnO, $CuCrO_2$, Annealing steps, Carrier Concentration, Transparent P-N Junctions

RESUMO

A eletrónica transparente tem recebido uma grande quota da investigação tecnológica, devido à demanda continua por melhores produtos devido à sua utilização em quase todos os produtos do dia-a-dia da sociedade moderna. Este trabalho vem explorar dois dos pontos fundamentais para a evolução desta tecnologia, a substituição do 'indium-tin-oxide' (ITO) por outro oxido condutor transparente e a introdução de um bom oxido condutor transparente do tipo p. Os materiais estudados para este efeito foram o ZnO e o $CuCrO_2$ que foram ajustados para uma grande quantidade de concentração de portadores, através de alterações de parâmetros de deposição e de processos de recozimento. Os filmes de ZnO mostraram um amplo alcance de concentração de portadores desde $8 * 10^{19}$ até $10^{18}\ cm^{-3}$, e até valores acima de $10^{20}\ cm^{-3}$, no caso dosfilmes dopados de Aluminio. Uma relação importante descoberta durante este trabalho foi a relação direta entre a mobilidade e a concentração de portadores, $\mu \propto n$, que se manifestou entre $10^{18} - 3 * 10^{19} cm^{-3}$. Filmes finos de $CuCrO_2$ mostraram também um grande alcance em termos de concentração de portadores desde $2 * 10^{21}$ até $10^{17}\ cm^{-3}$, mostrando um aumento progressivo da transmitância ótica desde 37% até 60% com a diminuição na concentração de portadores o que torna os filmes mais aplicáveis à eletrónica transparente. Uma junção P-N foi proposta com estes materiais com um alinhamento de banda tipo-II projetada e otimizado para uma concentração de portadores de $5 * 10^{18}\ cm^{-3}$, em ambos os lados da junção. A junção foi padronizada por etching e fotolitografia, mas infelizmente a concentração de portadores utilizada não foi a otimizada o que induziu um contacto óhmico.

Keywords: ZnO, $CuCrO_2$, Recozimento, Concentração de Portadores, Junção P-N transparente

Abbreviation List

ALD – Atomic Layer Deposition
AZO – Aluminium doped zinc oxide
CVD – Chemical Vapour Deposition
FTO – Fluorine Tin Oxide
GGA - Generalized Gradient Approximation
ITO – Indium Tin Oxide
LED – Light Emitting Diode
KPFM – Kevin Probe Force Microscopy
MOCVD – Metal Organic Chemical Vapour Deposition
MOSFETS - Metal Oxide Semiconductor Field Effect Transistor
PBE – Population Balance Equation
PL – Photoluminescence
SEM – Scanning Electron Microscopy
TFT – Thin Film Transistor
TCM – Transparent Conductive Material
TCO – Transparent Conductive Oxide
UV- Ultraviolet
VB – Valence Band
VBM – Valence Band Maximum
XPS - X-ray photoelectron spectroscopy

Symbols List

e - Electron charge
I – Current
I_{ON} – Current when diode is in ON state
I_{OFF} – Current when diode is in OFF state
n – Ideality factor
k – Boltzmann constant
s – Second
V – Electrical Potential
T – Temperature
σ - Conductivity
μ - electron mobility
n - Carrier concentration n-type
p – Carrier concentration p-type
Φ - Workfunction

Table of Contents

List of Figures

List of Tables

1 Motivation and Objectives

Transparent electronics is one of the technological areas with highest economic importance and still a good development margin, with every year costumers demanding better products, and enterprises and industries trying to overcome their competitors with newer capabilities. Transparent electronics is used by everyone in displays and sensors in every corner of modern day society. Its further development is however hindered nowadays by two crucial issues. One important piece that is still missing in the material portfolio of transparent conductors is a good transparent p-type transparent conducting oxide (TCO) that could permit full usage of pixels with introduction of fully transparent electronics, the introduction of photovoltaic windows and another panoply of fully transparent applications. The other problem is the expected shortage of Indium, as well as its inflated cost and toxicity, and so the need to find a substitute to the commonly used indium-tin oxide (ITO), that is still the mostly used TCO[1].

This work comes with the goal to explore ways to achieve these missing building blocks. The following objectives were investigated during the internship:

- Study of ZnO deposited by Atomic Layer Deposition (ALD) as replacement of ITO, and explore the tunability of the films for microelectronics applications through changes in deposition temperature and annealing conditions, with particular attention to the carrier concentration variation and mobility and study the interplay between them.
- Study of $CuCrO_2$ deposited by Metal Organic Chemical Vapour Deposition (MOCVD) in the group as p-type TCO, and study ways to tune the carrier concentration and to increase the optical transmittance of these films, to be suitable for several microelectronics applications.
- Development of a vertical P-N junction using both the materials such as suggested in Figure 1, with a top and a bottom contact. The patterning of the junction will be processed with optical lithography and wet etching. For this junction, the important challenge of n-type and p-type TCOs is to obtain a reduced carrier concentration while keeping a high mobility on both sides in order to optimize the rectification properties.

Completely transparent P-N junctions would permit the introduction of energy harvester windows, development of good UV emitters and detectors and transparent CMOS transistors enabling the use of full pixels in displays.

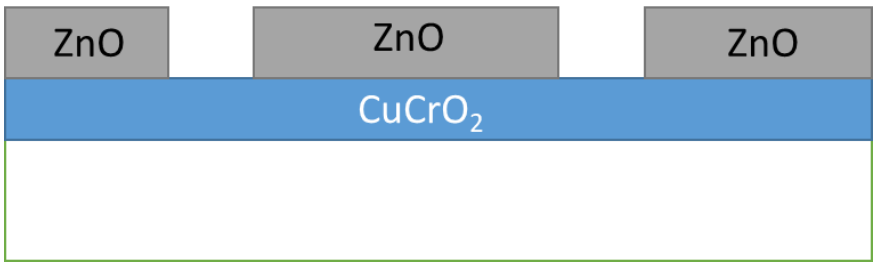

Figure 1 – Cross-section scheme of the projected P-N junction with a top and bottom contact

2 Introduction

TCO layers have been one of the biggest research focus in the recent years, due to their wide use in optoelectronic devices, from transparent electrodes in displays to Light Emitting Diodes (LEDs) or photovoltaic cells. TCOs are a special kind of materials that combine high electrical conductivity and large optical bandgap[1,2]. The extensive research is focused on finding a substitute to ITO as well as overpassing the lack of a good p-type TCO, that would enable the building of a transparent P-N junction[1]. Here we investigate in more details two potential candidates, ZnO as a replacement of ITO, and $CuCrO_2$ as p-type TCO.

2.1 - Zinc Oxide

ZnO is a direct bandgap semiconductor (Eg=3.3eV) with a large exciton binding energy (60meV) at room temperature [1,3–5]. The most common structure of ZnO is the wurtzite hexagonal structure[6]. ZnO films have received particular attention because of good electrical and optical properties (transmittance above 80% in the visible region [7]), high electrochemical stability, good resistance against Hydrogen plasma and low fabrication cost compared with indium-tin-oxide (ITO), placing it as a great candidate for industrial applications [3,5,8].

ZnO has been studied in diverse structures and with several different deposition techniques, as detailed by Ozgur et al.[9]. These films can be used for several applications from transparent electrodes (in particular for Aluminium doped Zinc oxide (AZO) films) , light emitting diodes, solar cells, gas sensors and bulk acoustic wave devices or transparent conductive coatings [2,5,6,8].

The wurtzite structure of ZnO is favoured by a (002) crystal orientation in most of high temperature techniques. This is because (002) orientation has the highest atomic packing density and the minimum surface free energy. Therefore the c-axis orientation is the most thermodynamically favourable growth of ZnO structure[10]. The crystal orientation can be important when it is used as nanostructures, such as vertically aligned nanowires[10–12].

In order to have thin films that can supply micro and nanoelectronics, with precise control of film thickness, conformality and morphology while keeping compatibility with low temperatures (less than 200ºC) for transparent and flexible electronics, Atomic Layer Deposition (ALD) as an interesting candidate. A binary introduction of fluxes separated by a purge step permits layer-by-layer control of deposition through self-limiting surface reactions[5,13]. Deposition temperature[4,14], purging time[15] and introduction of dopants[2,5,16] have been shown to modify the films properties. Electrical characteristics show an increase in resistivity with the decrease of deposition temperature [4,16]. At deposition temperature below 100ºC, the films have less preferential orientation and are more amorphous than the films deposited at higher temperatures, which show polycrystalline films with preferential orientations on (100), (002) and (101) planes[13,14,17]. Concerning the optical properties, lower deposition temperature films show higher transmittance in the visible region [14]. This allows ALD deposited films to have a wide variation of properties depending on the chosen conditions, what makes ALD a very interesting solution for deposition of thin-films. For thicker films the small growth rate (typically 0.18-0.20 nm/cycle for ZnO [18]) is a very limitative factor.

Functional properties of ZnO are determined in great part by the inclusion of intrinsic defects during the growth process. These defects contribute mainly to the electrical and luminescence properties of the films. In ZnO films deposited by ALD with no extrinsic defects, intrinsic defects are zinc interstitials, oxygen vacancies and hydrogen, acting as shallow donors [4,19–21]. It is known that the Fermi level is affected by the presence of these defects that is

supported by Kevin Probe Force Microscopy (KPFM) measurements and that these measurements can give an important information about the doping profile[22].

ZnO films present a strong ultraviolet emission that can be applied for optoelectronics, ZnO usually has two photoluminescence (PL) peaks centred in green (2,38eV) and in Ultraviolet (3,18eV). The green peak is assumed to be caused by the intrinsic defects presented before.[23–25] It is believed that the increase of green peak is related to increase of zinc interstitials and oxygen vacancies. The ultraviolet (UV) emission peak corresponds to the exciton transition.[23,24]

In order to improve the electrical properties to be able to compete as a transparent conductive oxide (TCO) with ITO, ZnO has been doped with group-III elements[11,25,26], among them Al-doped ZnO films show great potential as TCO and for transparent electrode purposes with high mobility and very low resistivity. Several studies point out for a maximum mobility as well as maximum optical transmittance films at 3 at. %[5,26]. For thin films with higher Al concentration it is shown a strong decrease of the conductivity as well as an abrupt increase of the optical bandgap, that can be justified by the appearance of Al_2O_3 phase [5,27]. Therefore, AZO and ZnO films can play a significant role substituting ITO as the main n-type TCO as well as fulfilling many other roles in optoelectronics as a semiconductor layer.

2.2 - Copper Chromium Oxide

A tremendous amount of research has been applied with efforts focusing on finding a p-type material with properties matching the widely used n-type TCOs. , AMO_2 (with A = Cu or Ag and M = Al, Sc, Cr, Fe, Ga, or Y) with the delafossite structure, have received a lot of focus on research as a potential TCO, with very promising electrical and optical properties. Still these materials are running orders of magnitude behind in terms of conductivity when compared with n-type TCOs[28,29]. The highest conductivity of 220 $S.cm^{-1}$ was reached for Mg doped $CuCrO_2$ [30], although this value is not confirmed by further studies. Special attention has been given to $CuMO_2$ materials due to their expected large hole mobility resulting from the interaction of Cu 3d states with O 2p states, similar to the interaction in Cu_2O where the valence band is dominated by Cu 3d states [28,31]. Cu_2O has a narrow bandgap (2,17eV) while $CuMO_2$ materials present a much wider bandgap (above 3eV) by introduction of this large radius metal while keeping the high conductivity[28–32].

In the delafossite each Cu atom is coordinated with two oxygen atoms, forming O-Cu-O dumbbells parallel to the c axis. Oxygens are coordinated with three M^{III} atoms as shown in Figure 2 which can lead to two structures, a rhombohedral (Figure 2.1 a)) or hexagonal (Figure 2.1-b)) unit cell [32,33]. In this material, the hole conduction is believed to be through small polaron hopping mechanism. Although Cu-based delafossites have shown high mobility values for p-type semiconductors (up to 1 $cm^2 V^{-1} s^{-1}$) [31,34–36], it is complicated to increase these mobility values with this conduction mechanism[35].

Copper chromium oxides have advantages compared to other delafossites in terms of high density of states of 3d M cations originated by Cr^{3+} near the valence band maximum permitting good hole mobility, covalent mixing between oxygen and chromium ions and good dopability, that is most efficient with Mg, Fe, N_2 or Zn that allow great conductivity increase. These advantages make $CuCrO_2$ a perfect candidate for p-type TCOs[29,32]. Still it is to notice that compared with $CuAlO_2$ it usually presents lower transmittance[37]. Mg is the most common way of doping $CuCrO_2$, and as shown by Chikoidze et al.[38], increasing Mg content will decrease oxygen vacancies and so enhance hole concentration, up to a maximum at 5% Mg. The same work shows an increase in conductivity up to 3 orders of magnitude with Mg concentration of 4.7%. One question still under intense debate regarding the $CuCrO_2$ is the conduction mechanism with both Cu^I/Cu^{II} and Cr^{III}/Cr^{IV} being proposed[29,32,39]. This question arises mainly

since the change of M cation changes the conductivity by several orders of magnitude, thus showing the importance of this cation in the conduction properties. On the other hand the Cu_I/Cu_{II} states seems to dominate the valence band maximum (VBM) as demonstrated by X-ray photoelectron spectroscopy (XPS) studies[39], generalized gradient aproximation (GGA) calculations[39] and population balance equation (PBE) simulations[40], thus favoring the Cu hole mechanism[39]. It is predicted that the increased of the conductivity of delafossite with Cr in the M site is due to the mixing of Cr d states with Oxygen 2p states in the valence band (VB), producing shallower transition level for the Cu-based holes[39,40].

There are several methods reported to produce CuCrO2 which include, solid-state reaction[41], sol-gel[42,43], pulsed laser deposition[44], magnetron sputtering[45] and CVD[46]. Usually these techniques require high temperatures that are incompatible with transparent electronics. A possible solution that was studied by J. Crêpellière et al.[29] uses metal organic chemical vapour deposition (MOCVD), to promote the growth of $CuCrO_2$ thin films using direct liquid injection (DLI) CVD in a one step process. This solution allows using temperatures as low as 330˚C, more compatible with transparent electronics. As it is shown in Figure 2.2, it allows large conductivity (up to 17 S cm^{-1}) and lower temperatures at the cost of lower average transmittance in the visible region[29]. These results show the potential of delafossite $CuCrO_2$ thin-films when considering the fabrication of transparent P-N junctions particularly suitable for electrical rectification or photodetection purposes.

An intensive study of the deposition characteristics of $CuCrO_2$ by DLI-MOCVD was performed by Lunca Popa et al.[28], showing promising values with deposition temperatures of 450ºC presenting conductivities up to 100 S.cm^{-1} [28] and carrier concentrations of $10^{21} cm^{-3}$ without any extrinsic defect doping and with pure phase $CuCrO_2$.

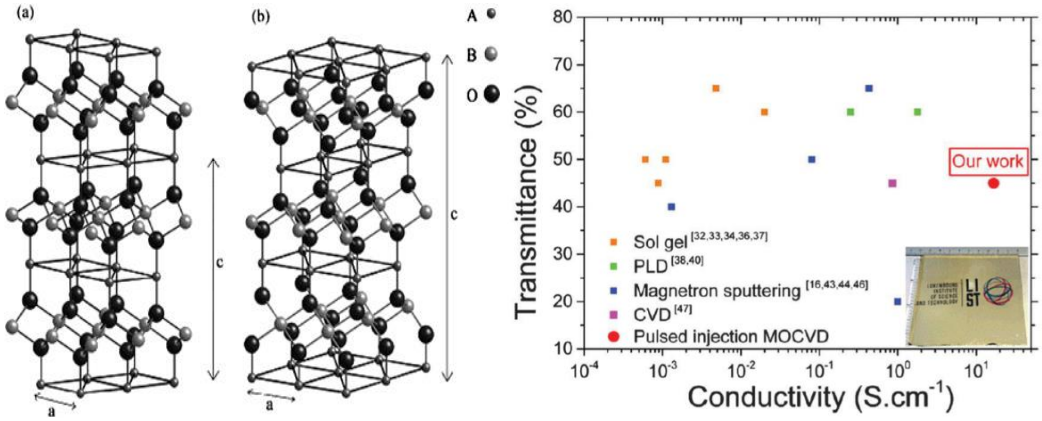

Figure 2 - 2.1- Delafossite structure (a) 3R polytype, R3¯m space group symmetry (rhombohedral unit cell); (b) 2H polytype, P63/mmc space group symmetry (adapted from Marquardt et al.[33]); 2.2 - Comparison of the conductivity and the optical transmittance of MOCVD studies developed in J.Crêpellière et al.[29] with past literature work with different deposition technique, showing the high conductivity of samples deposited in LIST by MOCVD compared with the past works.

2.3 - Annealing of TCOs

These materials arise new possibilities not only as a promising candidate in the case of ZnO to become a common TCO, but mostly their combination might permit to create an all-new kind of optoelectronics, enabled by a fully transparent P-N junction.

In order to create this junction there are factors that need to be taken into consideration: the control of the carrier concentration, maximization of carrier mobility, optical properties and minimization of interface leakages. These parameters can be achieved mainly by changing the deposition conditions or by post-annealing treatment[47]. Annealing the ZnO can change several properties such as the morphology, with works claiming improved crystallinity in annealed ZnO

films[48], and mostly the electrical properties with a great change in conductivity depending on annealing temperature and time[4,25,26]. Annealing seems to be an interesting way to control the conductivity, through changes in carrier concentration, and mobility of ZnO making it able to provide the wide range of applications it has been projected for. Figure 3.1 exemplifies this with the variation of mobility and carrier concentration with different annealing temperatures. Literature shows an increase in grain size occurs with annealing temperatures higher than 500ºC. Up to this temperature, the gain size is shown to be kept mostly constant[25].

With the potential arise of these capable p-type TCO and in order to produce a good P-N junction one need to study ways to tune the ZnO for lower carrier concentration, but that can conserve the high electron mobility (expected μ = 15 ~ 60 cm^2/Vs) [2,5]. As shown in literature this can be quite hard to achieve since there appears to be an intrinsic tendency in intrinsic Zinc Oxide to have a decrease of mobility with decrease of carrier concentration [49–51]. The mobility of ZnO and doped ZnO films is believed to be dominated by ionized impurity scattering when the carrier concentration is in the range $10^{20} - 10^{21}\ cm^{-3}$. It thus mainly concerns doped ZnO films (e.g. AZO). Below this carrier concentration, both the ionized impurity scattering and the grain boundary scattering need to be taken into account.[52] According to the past works, there is a peak of mobility that can be found in ZnO close to carrier concentrations of the order of 10^{20} cm^{-3}, like is seen in Figure 3.2, where grain boundary scattering decreases and is still not overcome by ionized impurity scattering [2,5,47,52].

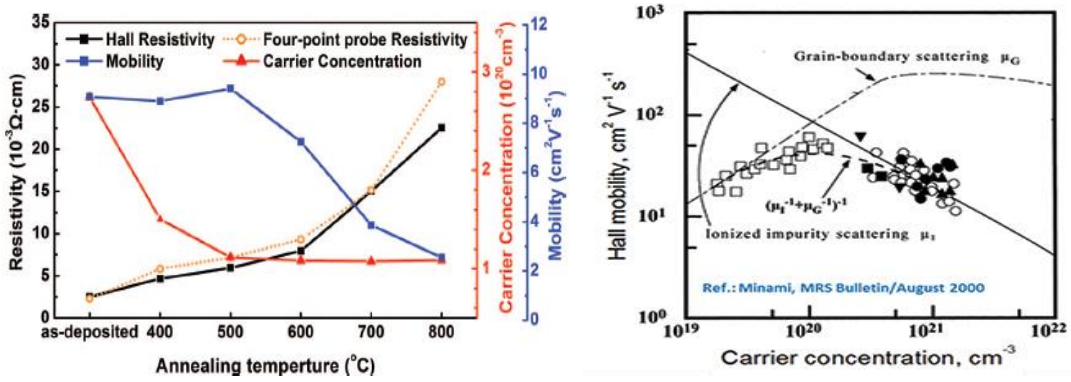

Figure 3- 3.1 - Resistivity, carrier concentration, and Hall mobility as a function of annealing temperature for AZO films deposited on SiO_2 substrate - adapted from Geng et al. [25]; 3.2 - Hall Mobility as function of carrier concentration showing the different scattering regimes, by Minami et al.

The annealing atmosphere is still under debate with several works pointing in different directions, and even some of them claiming to have an increase of the conductivity and of the carrier concentration with annealing processes conduced in Vacuum[53] and N_2[54] for ZnO films without extrinsic doping. Still most of works point out to a decreasing carrier concentration in any atmosphere with increasing time and annealing temperature. Table 1 summarize some of the works on the annealing of ZnO with different conditions.

Table 1 - State of the art of ZnO annealing atmospheres

Article	Gases Used	Considerations
Jin et al.[51]	Air	Decrease in carrier concentration with temperatures from 160-280° - time range from 20 to 120 minutes.
Wang et al. [26]	Ar, N_2 and Air	Two hours annealing at 350ºC. Show better control and less decrease in mobility in Argon annealing.
Laube et al. [4]	Vacuum and O_2	Similar results in carrier concentration but doesn't study mobility effect. Study from 150 to 500ºC.

Lin et al. [55]	N_2	Study from 400º to 700ºC showing a major decrease in carrier concentration at 500ºC for 45 minutes.
Kennedy et al. [53]	Vacuum and air	Carrier density increases in vacuum for 30 min annealing at 500ºC. In air, there is a 4 order of magnitude decrease with same annealing conditions.
Geng et al. [25]	O_2	Decrease in carrier concentration without big decrease in mobility up to 400ºC. Above this temperature there is a major decrease in mobility.
Lu et al. [54]	O_2 and N_2	Sequential annealing steps show that N_2 leads to a decrease in resistivity and O_2 to an increase

The optical transmittance of the films seems to be stable under different annealing conditions up to 500ºC [25,26,56].

Like the zinc oxide the delafossite films can also be tuned for the application by thermal annealing, although they require much higher temperature, according to the work of Götzendörfer et al.[37], at least 620ºC are required to measurable difference in electrical characteristics of delafossite films, what can suggest a higher activation energy of the present defects. Annealing in delafossite above this temperature is shown to reduce the carrier concentration and increase transmittance values in the optical region of 20% [42,45,57], as well as increase of crystallinity and acquisition of pure phase $CuCrO_2$ in case of existence some parasitic phases, such as CuO, CuO_2 and $CuCr_2O_4$[29,37,45,57]. The evolution of the mobility with post-thermal annealing is not quite understood with measurements from Seebeck coefficient showing a decrease in carrier mobility with any annealing temperature, but then a gradual recovery of mobility with further increase of annealing temperature. Optical bandgap of delafossite seems not to be affected by annealing processes[42]. Still in the literature there is a lack of quantitative studies, when it comes to $CuCrO_2$ without extrinsic doping, on the influence of the annealing processes on the electrical properties of the films.

2.4 - Transparent P-N junction

Many wide bandgap semiconductors have been explored to form a transparent p-n junction. Since most TCOs are unipolar, challenges exist in creating a heterojunction that combines a good band alignment with a good electrical response. Simple p-n junctions can derive into photodetectors and photovoltaic cells and can open paths into the transparent transistors. Extensive works have been realized in recent years trying to find a good transparent p-n junction as shown in the review report by Grundmann et al. [49], with special emphasis on a NiO-ZnO heterojunction that lead to good electrical responses. It is shown by past works that type-II band alignment could be one of the most favourable for the good function of the junction since forward current is usually due to interface recombination and the injection of minority carrier is negligible. This is the band alignment predicted for the $CuCrO_2$-ZnO heterojunction.

3 Materials and Methods

$CuCrO_2$ films were deposited by MOCVD using Direct Liquid Injection - Metal Organic Chemical Vapour Deposition system DLI-MOCVD, (MC200 from Annealsys), which is a stagnation point-flow warm-wall reactor. The used copper and chromium precursors are bis[2,2,6,6-tetramethyl-3,5-heptanedionato] copper(II) and tris[2,2,6,6- tetramethyl-3,5-heptanedionato]chromium(III), respectively ($Cu(thd)_2$ and $Cr(thd)_3$, Strem Chemicals). Cyclohexane solutions with a total precursor concentration of $[Cu(thd)_2] = [Cr(thd)_3] = 2{,}5mM$ were used. The total canister solution used was 1 L of Cyclohexane with 1.075 g Cu(thd) +1.5 g Cr(thd). The deposition parameters used were: substrate temperature of 450 °C; oxygen flow used was 2000 sccm; nitrogen flow of 850 sccm and the total process pressure was 12 mbar. The process used followed the previous optimization detailed by Lunca Popa et al.[28].

ALD deposition of ZnO and Al:ZnO followed the process described by Roge et al.[58], using in our case Argon as purge and carrier gas, for 500 cycles and with a pulse sequence:1 - Diethylzinc (DEZ, $Zn(C_2H_5)_2$) pulse 150 ms; 2 - purge 10 s; 3 - H_2O pulse 200 ms; 4 – purge 10 s. In the case of the AZO at each 30 cycles it was used a pulse of Trimethylaluminum (TMA, $Al(CH_3)_3$).

All the annealing processes were performed on a Rapid Thermal Annealing reactor (Annealsys), at low pressure, using in the case of $CuCrO_2$ films a nitrogen flow of 500 sccm and in the case of ZnO a nitrogen flow of 25 sccm. The annealing curve was first a heating ramp with 5 ºC/s, a waiting time at constant peak temperature and a cooling ramp with -5 ºC/s. The varied annealing time was the waiting time and the heating and cooling times are not counted.

Prior to ALD deposition the glass substrate was previously cleaned in acetone and ethanol and dried with nitrogen jet.

All the measurements were carried out at room temperature.

Electrical measurements were made using Hall effect Measurement Ecopia HMS-3000 with a magnet of 0,562 T using van der Pauw configuration for extracting the carrier concentration and the mobility (in the range between $1 - 10^7 \frac{cm^2}{Vs}$). The sheet resistance is first measured in van der Pauw configuration without any magnetic field applied, that permits to calculate the conductivity, and then the Hall voltage is measured with a magnetic field, from which we calculate the carrier concentration. The mobility is extracted as shown in equation 1.

$$\sigma = e(\mu_e n + \mu_h p) \qquad \text{(equation 1)}$$

In all cases we assume that there is only one type of carriers (majority carriers). We have checked that the majority carriers in ZnO are electrons, and in $CuCrO_2$ majority carriers are holes. We thus neglect the cases where the two carriers can contribute to conductivity, which can potentially result in a miscalculation due to compensation doping.

Mobility measurements are expected to have an error up to 30%, considering an error up to 10% of the 4-Point-Probe measurements and up to 20% in the carrier concentration, coming from a 10% error in the thickness measurement from elipsometry and a 10% error in the Hall resistance measurements.

In addition to the Hall effect measurement, 4-Point-Probe measurements were realized on a Jendel Cylindrical four-point linear probes head with a Keithley Source Meter 2614B to extract the sheet resistance of the films according to equation 2.

$$Rs = 4.532 * 0.925 * \frac{V}{I} \qquad \text{(equation 2)}$$

The mobility of $CuCrO_2$ films are too low for the Hall effect measurement system, we performed Seebeck coefficient measurements on a homemade system with a copper wire as

reference. In this system, copper blocks are thermally separated one is heated, while the other is kept at room temperature. With this there is a small voltage build-up, this difference in voltage vs. the difference in temperature can be plotted. From the fit of the slope we calculate the Seebeck coefficient, as shown in equation 3. An example of the plot used to extract S is shown in Figure 4, showing the different slopes associated with p and n-type semiconductors.

$$S = -\frac{\Delta V}{\Delta T} \quad \text{(equation 3)}$$

Photoluminescence measurements were realized on a Renishaw inVia microspectrometer using a grating of 300 gr/nm, an objective of 15 times UV (Thalabs) and with laser power of 100% corresponding to 8mW and using two lasers a UV and blue one with corresponding 325nm and 442nm wavelength. Transmission and reflectance spectrum were acquired in the range from 1500 to 250nm using a Perkin Elmer LAMBDA 950 UV/Vis/NIR Spectrophotometer with a 150 mm InGaAs Integrating Sphere.

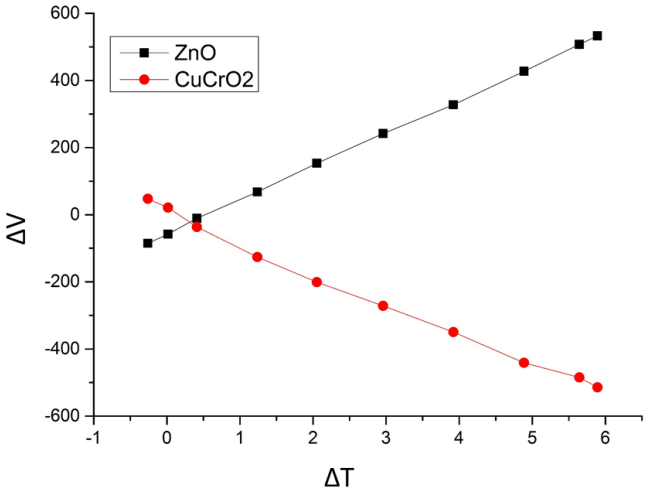

Figure 4 - Plot of the variation of voltage as function of variation of temperature that permits the extraction of Seebeck coefficient and showing the different behaviour between p-type ($CuCrO_2$ deposited at 450ºC) and n-type materials (ZnO deposited at 200ºC)

The structure of the grown films was studied by X-Ray Diffraction (XRD), Bruker D8 Discover, using monochromatic Cu Ka radiation (l = 1.54 Å) at 40 kV and 40 mA. The analyses were performed using the θ/2θ configuration from 25 to 50º at a scanning step of 0.02º and with 3s/step. Kevin Probe Force Microscopy (KPFM) measurements have been performed on a Bruker Innova using the surface potential mode as amplitude modulation. Surface topography is obtained in the first pass and the surface potential is measured on the second pass. Freshly cleaved highly-oriented pyrolitic graphite (HOPG) is used as reference. The measurements are performed under dry N_2 atmosphere to avoid contaminations on the surface. The surface morphology of the films was inspected by Scanning Electron Microscopy (SEM) with 10kV of acceleration voltage, FEI Helios Nanolab 650 with EDX spectrum analysis connected to SEM Oxford Instrument Xmax 50mm^2 with the previous acceleration voltage. Thickness of the $CuCrO_2$ films was measured using the same equipment with a cross-section view on silicon.

The thickness of the ZnO films was measured on a Si wafer beneath the samples using ellipsometry M2000J.A. Woollam Co with a Si + Native SiO_2 + ZnO model.

Dry etching was processed on PLASMATHERM 790 Reactive Ion Etching chamber using CF_4+Ar gases and with 500W RF Power. It was used a bi-layer of LOR3A with 300 nm and on top a Shipley S1813 with 1.2 µm, spin-coated for 1 minute at 4000 rpm and with an acceleration of 1000 $\frac{rpm}{s^2}$, both baked for 1 minute at 115ºC. For the wet etching process was prepared a

single layer of ShipleyS1813 with the previous conditions. It was used on both etching cases HDMS as a promotion adhesion that was spin-coated at 4000 rpm for 30 seconds with an acceleration of 1000 $\frac{rpm}{s^2}$, baked for 1 minute for 115ºC.

The lithography was processed on a Heidelberg Instruments MLA 150 with the pattern shown in Figure 5, with circular patterns with 3 different radii, 250, 500 and 1000 µm. It was run a dose test and used 90 $\frac{mJ}{cm^2}$. After exposure, the samples were developed using a MF319 for 40 seconds and after rinsed for 30 seconds. The samples were dipped in $FeCl_2$ where several solutions were tried favouring the used one at 0.1% for 15 seconds. The samples were then cleaned in acetone for 2 minutes for photoresist removal. The images of the samples were taken using Leica DFC295 microscope.

For electrical characterization of the junction was used a configuration with 2 points at different voltage, with a voltage sweep and measuring the current between the two tungsten tips, as shown in Figure 6. The Sweep tip was kept on the $CuCrO_2$ contacted with silver paste and the constant -0 V was kept on ZnO pads.

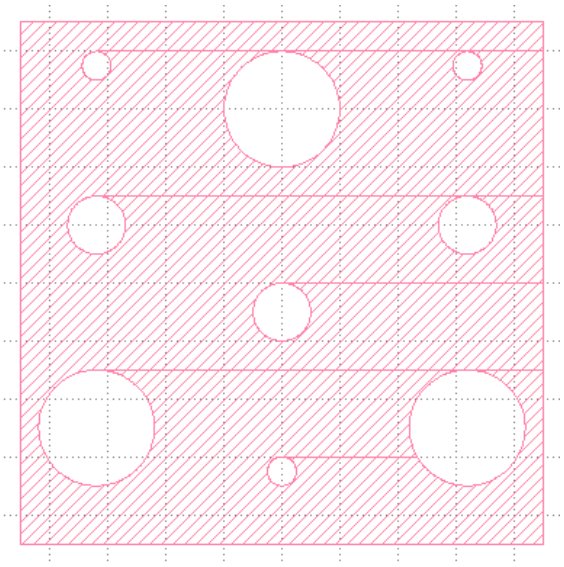

Figure 5 - Layout of the mask used with nine patterns with diferent radii, 1000, 500 and 250µm.

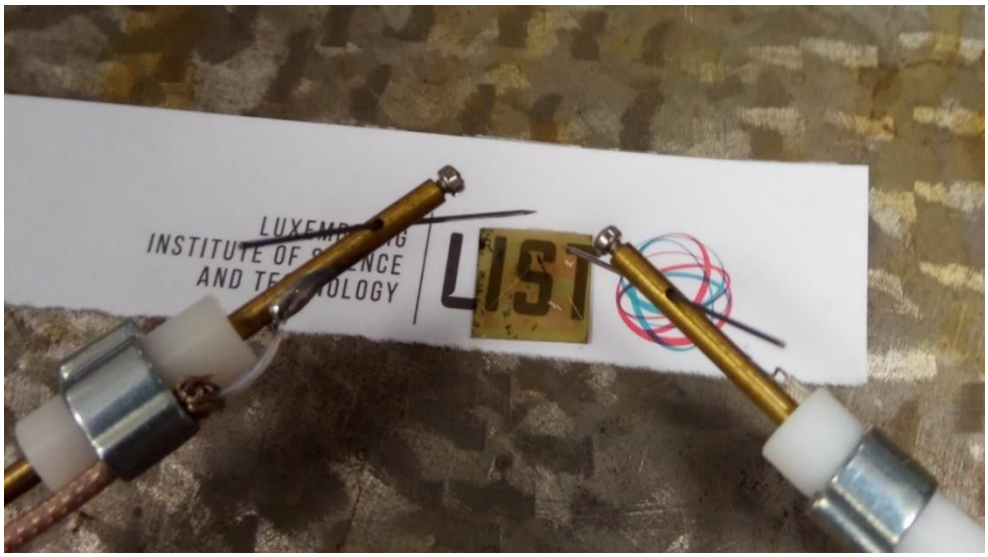

Figure 6 - Photography of the junction with the 2 points used for I-V traces

4 Results and Discussion

4.1 ZnO

The Study of the ZnO was proposed with the objective of studying the influence of the deposition temperature on the carrier concentration and study ways to further decrease this carrier concentration for transparent microelectronics applications while keeping a high mobility. The relationship between the mobility and the carrier concentration was more particularly studied. For this purpose, we performed three depositions by ALD at different temperatures. These films were consequently annealed studying the influence of the atmosphere, the time and the temperature. XRD tests were run to study the crystallite size and SEM to confirm the morphology. PL was studied to see the impact of the annealing on the excitonic peak.

4.1.1 ALD deposition temperature study

Table 2 - Electrical parameters of ALD deposited ZnO at 130°, 150º and 200°C, with error bars from statistical analysis from 8, 12 and 19 samples respectively.

Deposition Temperature	*130°C*	*150°C*	*200°C*
Carrier Concentration (cm^{-3})	$2.7 * 10^{19} \pm 6 * 10^{18}$	$5.1 * 10^{19} \pm 5 * 10^{18}$	$7.7 * 10^{19} \pm 8 * 10^{18}$
Mobility (cm^2/Vs)	16.4 ± 2.6	18 ± 0.9	22.6 ± 2.5
Conductivity (S/cm)	62.2 ± 12.8	126 ± 3.42	166 ± 47.9
Thickness (nm)	101 ± 10	121 ± 4	100 ± 9

The deposition temperature plays a significant role in the electrical properties of the films, as shown in Table 2. In the chosen temperature range, the growth rate by ALD is expected not to be independent on this temperature window[4,18]. However, while all three depositions were performed with the same 500 cycles, the thickness of the deposition at 150°C is bigger than the other two depositions. The main reason is a different configuration in the reactor being used for this particular deposition. On the other hand, almost no difference is seen between the depositions at 130 and 200°C, with a growth per cycle of 2 Å/cycle, in the expected ALD growth rate of 1.8-2.0 Å/cycle[18]. The most important result is the decrease in carrier concentration, in mobility and consequently decrease in conductivity of the films with the decrease in the deposition temperature. We further note that, under these conditions, the carrier concentration is still too high for use in active electrics applications. For this reason, we further studied an annealing step in order to decrease it.

AZO films were also deposited. The deposition was processed at 200ºC and resulted in films with a thickness of 84 nm, with an average carrier concentration of $4 * 10^{20}\ cm^{-3}$, and mobility

of 12 $\frac{cm^2}{Vs}$. These films are expected to have 3% Al content. Since AZO is intended for metallic-type transparent contacts, no further annealing was planned for this material.

4.1.2 Influence of annealing temperature, atmosphere and time on mobility and carrier concentration

Firstly, it was programmed an annealing with the 200°C deposited samples based on previous literature works, to have a deeper understanding of the influence of temperature, ranging from 300° to 450°C, atmosphere, using N_2 and argon during the annealing process and varying the time between 15 and 360 minutes. In annex 1 is presented the table with the electrical results and annealing plan of every sample.

In Figure 7 is presented the influence of the annealing atmosphere on the electrical properties: carrier concentration and electron mobility. It is possible to see the little influence on the electrical proprieties with the change in atmosphere between N_2 and Ar, with these slight changes falling in the associated error considerer for Hall effect measurements. With these conclusion, all annealing tests were further studied under N_2 atmosphere.

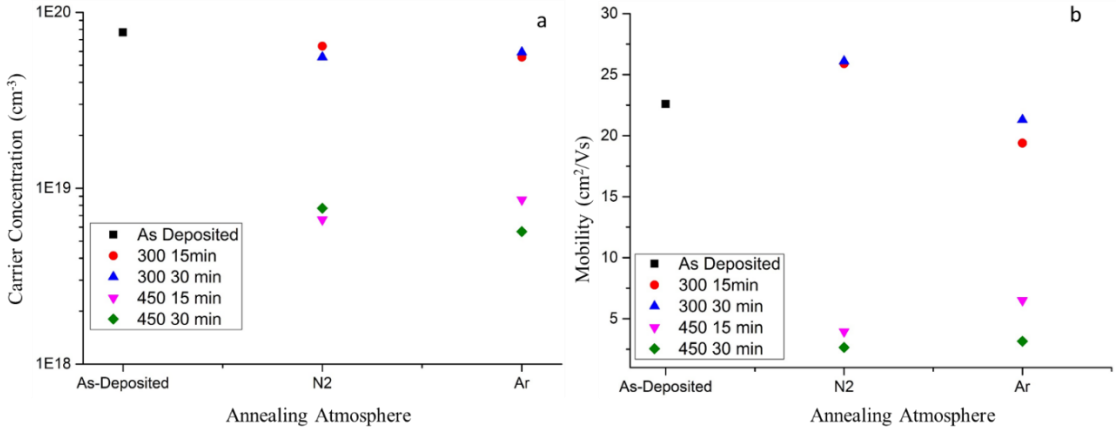

Figure 7 - Annealing studies with samples deposited at 200ºC, comparing the influence of the annealing atmosphere on the electrical properties with annealing at 300ºC and 450ºC for 15 and 30 minutes: - a) Carrier Concentration; b) Mobility

As shown in graphic 8. we see that the temperature has a strong influence over the carrier concentration with a severe decrease of the mobility. Annealing steps processed at 300ºC show very little impact on the initial values and with increasing temperature is shown a big decrease in carrier concentration. This suggests that the annealing temperature required for starting to heal defects on these samples deposited at 200ºC is above 300ºC, since with 350ºC there is already a factor of 4 times reduction in carrier concentration. The highest annealing temperature was 450ºC, to avoid changes in the crystalline structure of the ZnO, with this annealing showing a 10 times decrease when compared with the as-deposited samples, with 15 minutes annealing. The mobility is always impacted in a similar way showing a gradual decrease comparable with the decrease in the carrier concentration. The annealing time was seen to have much smaller impact in carrier concentration, with times from 15 min ($8.6 * 10^{18}\ cm^{-3}$) to 6 hours ($3.8 * 10^{18}\ cm^{-3}$) being studied. This 24 times increase in time resulted in a decrease in carrier concentration to about half the original value and a similar decrease in mobility. These samples presented a carrier concentration from $8 * 10^{19}$ cm^{-3} as-deposited and with 300ºC annealing to a minimum of $3 * 10^{18}$ cm^{-3} with annealings at 450ºC for 6 hours. The mobility of the films decreases from 26 to 2 $\frac{cm^2}{Vs}$.

It was studied another annealing plan for the samples deposited at 130° and 150°C, to further decrease the carrier concentration, in this case with samples deposited at another temperature.

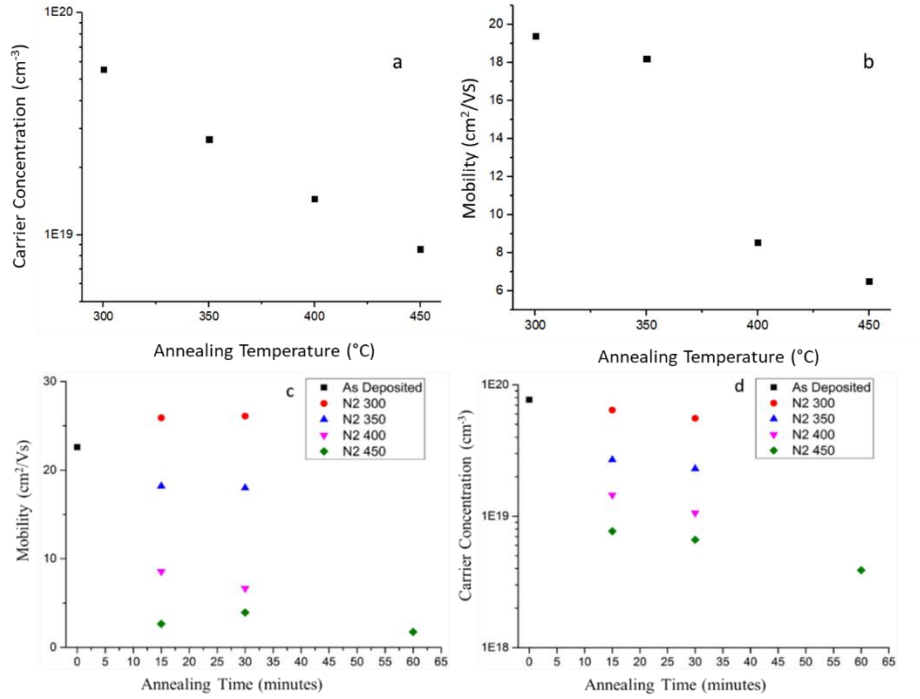

Figure 8 - Annealing with samples deposited at 200°C in order to study the influence of: - a) Annealing temperature on mobility; b) Annealing temperature on carrier concentration; c) Annealing time on mobility; d) Annealing time on carrier concentration

The samples with deposition temperature of 130°C presented after annealing very low carrier concentration and mobility values, what was a problem to be measured by this Hall-Effect system with accuracy, due to the range of mobility going only as low as $1\frac{cm^2}{Vs}$. The values of carrier concentration and mobility can thus not be extracted accurately using our system, and is preferred to analyse the resistivity measured by 4-Point-Probe. The resistivity change as a function of annealing temperature and annealing time are shown in Figure 9. Still it is possible to observe once again the strong increase of resistivity with the increase of annealing temperature and a small increase also in resistivity with the increase in time

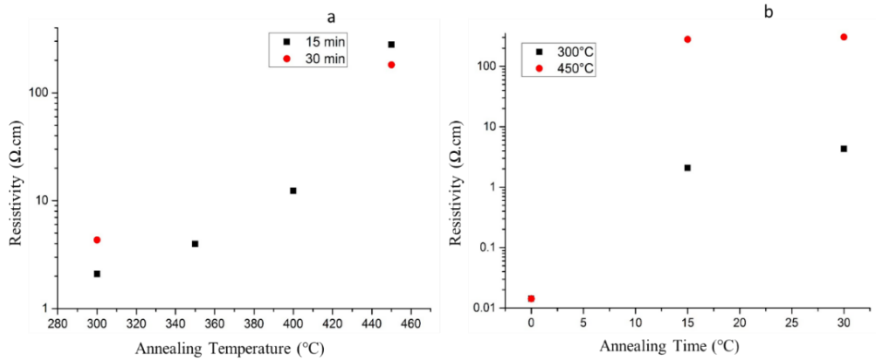

Figure 9 - Resistivity values resulting of annealing of samples deposited at 130°C as a function of: a) annealing temperature; b) annealing time.

Samples deposited at 150º were annealed from 150ºC to 450ºC for 15 minutes. At 300ºC was also made annealing steps with times of 30 and 60 minutes as well as at 450ºC was made an

annealing for 30 minutes. These samples have shown a wide range of tunability of carrier concentration from $2.6 * 10^{19} cm^{-3}$ to values approaching $10^{18}\ cm^{-3}$ as represented in Figure 10. Once again it is possible to associate a decrease both in carrier concentration and in mobility for the samples that were possible to measure with accuracy (annealing steps up to 350ºC).

To a bigger extend it is possible to associate the increase in resistivity with both the increase in temperature and in time as shown in Figure 11. Figure 12 represents all the samples annealed between 300 and 450ºC, it is presented with resistivity in order to compare samples with lower carrier concentration and mobility and in order to compare films with different thicknesses. We clearly evidence the increase of resistance of the films with the increase in annealing temperature, but also the low influence of the time in most of the cases. It is also shown that any annealing temperature above the deposition temperature on the samples deposited at 130ºC and 150ºC show a significant decrease in the carrier concentration leaving a big gap where it is hard to tune it precisely.

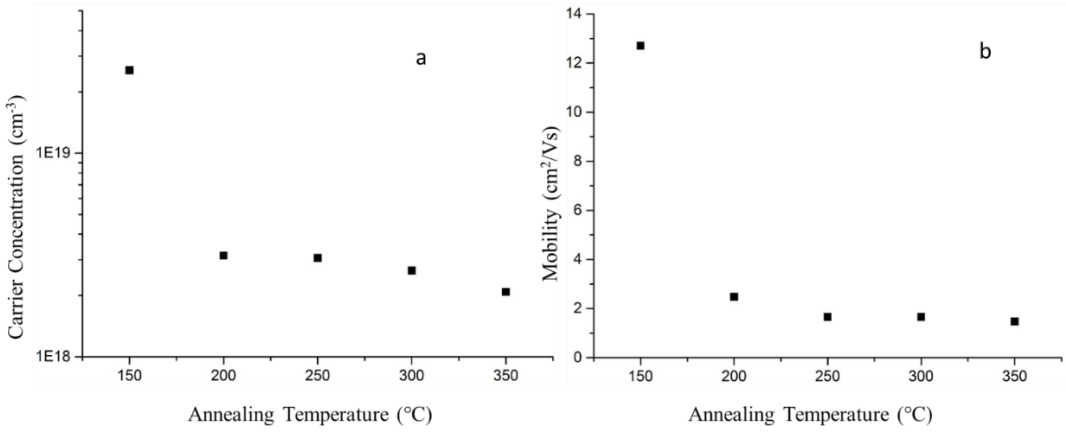

Figure 10 - Annealing studies of samples deposited at 150°C for 15 minutes: a) Carrier Concentration; b) Mobility as function of annealing temperature

Still as an overall between all the deposition temperatures and annealing performed it is possible to achieve any carrier concentration from below $1 * 10^{18}\ cm^{-3}$ to $8 * 10^{19}\ cm^{-3}$, as shown by Figure 13-a). Also in this graphic, we clearly observe a scaling low between the carrier concentration and the mobility. A fit of the data below the carrier density of $3*10^{19}$ cm^{-3} shows a linear relationship, $\mu \propto n$, as shown in the fitting made in Figure 13-b).

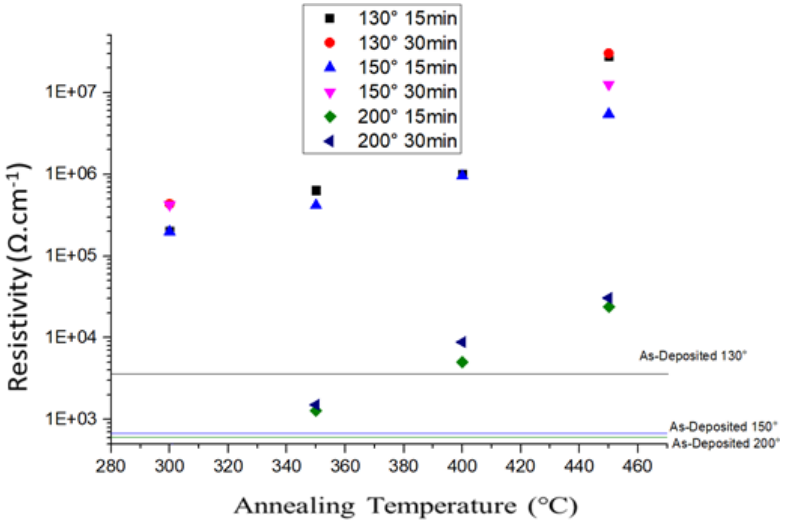

Figure 11- Resistivity study of samples deposited at 130,150 and 200°C with annealing temperatures ranging from 300° to 450°C and 15 and 30 minutes of annealing time

This scaling law is a major result that allows us to understand why the decrease in the carrier concentration by the effect of thermal annealing is always impacting the mobility. This is associated with the close relationship that they have due to the type of scattering mechanism never changes, what can be confirmed by XRD, to evaluate the difference in grain boundaries with annealing.

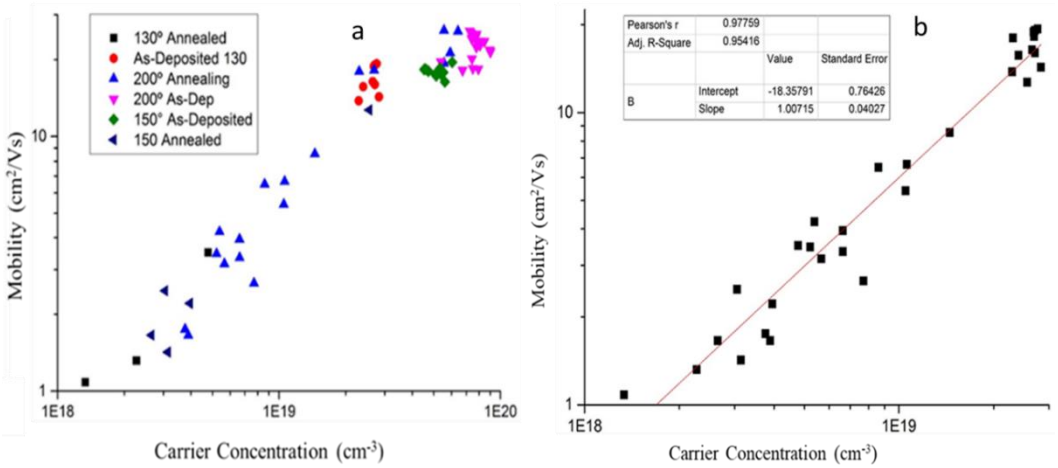

Figure 12 – a) Carrier Concentration vs Mobility of all ZnO samples as deposited and annealed. b) Fitting of the Mobility as function of carrier concentration for samples with carrier concentration from $10^{18}\ cm^{-3}$ *to* $3 * 10^{19}\ cm^{-3}$

From Figure 13-a) there are two main regimes, a first regime where there is a linear increase of the mobility with the increase in carrier concentration, that is explored in Figure 13-b) with the fitting, and another regime above $3 * 10^{19}\ cm^{-3}$ where there is a saturation of the mobility with the increase in carrier concentration. The first regime can be associated with the expected increase of mobility with the increase of the Fermi level for the grain boundaries scattering mechanism. Still with a further increase of carrier concentration, there starts to be an interplay between the grain boundary scattering and the ionized impurity scattering. The latest has an expected decrease of mobility with the increase in carrier concentration, what creates a region where mobility is stable for a small range of carrier concentration. This is in accord with previous works such as Minami et al. [52]. AZO films present a higher carrier concentration, $4 * 10^{20}\ cm^{-3}$ and follow this trend with a decreased mobility, $12\ cm^2/Vs$ as compared with the as-deposited ZnO thin films.

With the considerations made for the annealing time and temperature study, a model was proposed that could explain the carrier concentration behaviour of the films with different annealing steps.

Assuming that the kinetics of the chemical reaction corresponding to the annealing of doping defects is of first order, the electron concentration, n can be expressed as a function of annealing time, *t* in a general way as:

$$n(t) \approx N_d(t) = N_0 e^{-kt} + N_{res} \text{ (equation 4)}$$

where N_d is the donor dopant concentration, N_{res} is the residual acceptor concentration after infinite annealing, N_0+N_{res} is the initial carrier concentration (as deposited) and *k* is the rate constant.

We first check that the assumption of a first order kinetics is valid by fitting ln(n) vs. *t* for the data taken at 450°C. The reaction constant found was *k* $1.2 * 10^{-4} \pm 1 * 10^{-5}$ s^{-1}.

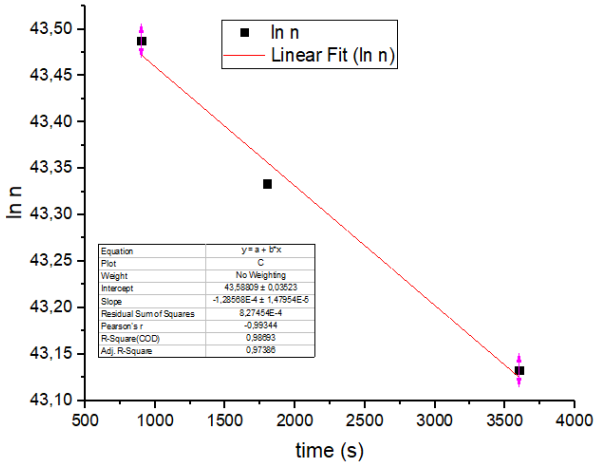

Figure 13 - Linear fit of ln(carrier concentration) vs annealing time for ZnO samples deposited at 200ºC and annealed at 450ºC

Assuming that the reaction is simply activated, the rate constant k can be expressed as a function of the annealing temperature T using an activation energy E_a:

$$k(T) = Ae^{-\frac{E_a}{k_B T}} \quad \text{(equation 5)}$$

where A is a constant and k_B is the Boltzman constant.

Relating equations (4) and (5), we can express the carrier concentration as a function of annealing temperature T and annealing time t:

$$n(T,t) = N_0 \exp\left(-At \exp\left(-\frac{E_a}{k_B T}\right)\right) + N_{res} \text{ (equation 6)}$$

In our case we can neglect in the fit the residual dopant concentration. In this case the relationship can be written:

$$\ln(\ln N_0 - \ln n(T,t)) = \ln(At) - \frac{E_a}{k_B T} \text{ (equation 7)}$$

Taking the "as deposited" carrier concentration as initial dopant concentration N_0 = $7.8 * 10^{19}$ cm^{-3}, we can plot $\ln(\ln N_0 - \ln n(T,t))$ at fixed annealing time t = 900 s as a function of $1/T$.

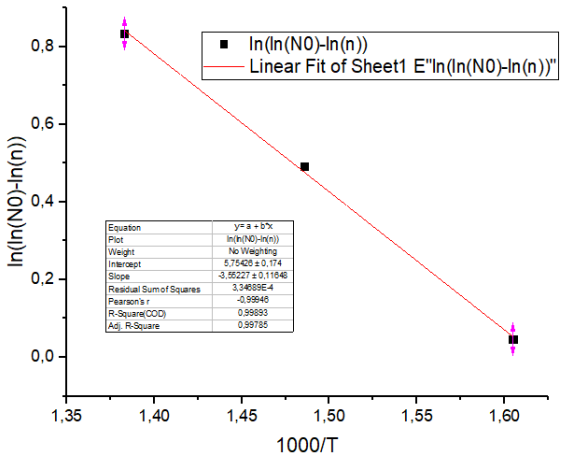

Figure 14 - Linear fit of ln(ln(N0)-ln(n)) vs 1000/annealing Temperature with ZnO samples annealed at different temperatures for a fixed time, 900s deposited at 200ºC

The data fit well with the activation energy model, and we obtain E_a/k_B = 3550 ± 100 K, E_a=0.31 ± 0.08 eV and ln(At) = 5.78 ± 0.17 (t = 450 s, A = 0.36 s^{-1}).

4.1.3 XRD

In order to explain the scaling behaviour between the mobility and the carrier density, we have assumed that the scattering mechanism due to grain boundaries does not change with annealing. In order to confirm this assumption, we have used XRD in order to estimate the crystallite size. Figure 16 represents a θ/2θ XRD spectrum of some of representative ZnO thin films. It is possible to see the peaks corresponding to the crystal orientations (100), (002) and (101), the most commonly ones associated with ZnO thin films. The main observation is the relative increase of the intensity of (002) peak on the samples deposited at 200ºC and annealed at 450ºC.

The lower boundary of crystallite size was studied from the FWHM extracted with the software 'intensity' and calculated with Scherrer equation (equation 8), where λ is the X-Ray wavelength, that in this case is 0,15 nm. The shape factor was assumed to be 0.9, a simplification made assuming the shape of the nanoparticles would be approximately spherical.

$$Crystallite\ Size = 0.9 * \frac{\lambda}{FWHM * cos\,\theta} \quad \text{(equation 8)}$$

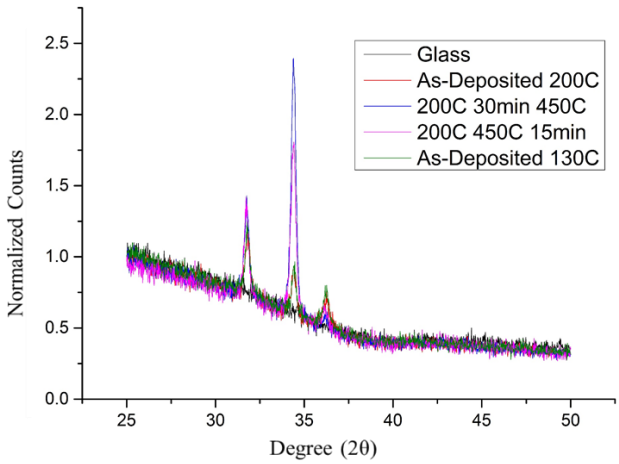

Figure 15 - XRD spectrum of ZnO thin films on θ/2θ configuration normalized to background

Table 3 - XRD analysis with crystallite size of each sample for each peak and the intensity of the given peak

Sample	Crystallite Size(nm) (100)	(002)	(101)	(100) Peak Intensity	(002) Peak Intensity	(101) Peak Intensity
200C - As Dep	25.97	26.83	26.83	83	64	30
130C - As-Dep	24.39	21.18	20.12	85	65	29
200C - 450C 30 min	26.83	25.97	19.17	143	425	26
200C - 450C 15 min	25.97	24.39	17.89	142	265	27

This increase of the crystallinity is associated with the annealing that in this case is both the highest annealing and deposition temperature, so with these conditions there seems to be a change in the preferential orientation, but it doesn't change the average crystallite size. Without

any significant change and mainly without a tendency of decrease of grain boundary when there is a decrease in carrier concentration, one can claim that the decrease in carrier concentration is most likely due to healing of defects during the annealing process and the decrease in mobility is associated with this decrease in carrier concentration and not in the increase of grain boundary in the film.

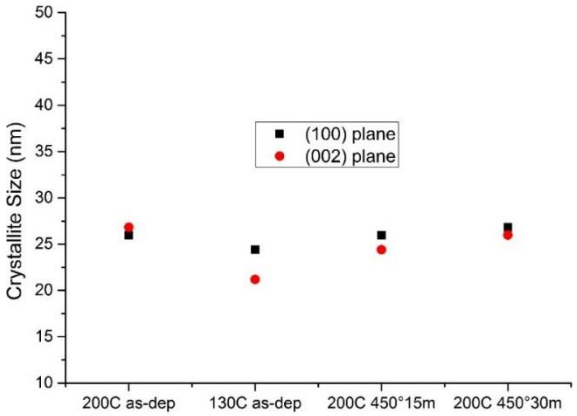

Figure 16 - XRD calculated Crystallite size on different samples for (100) and (002) planes

4.1.4 SEM

SEM analysis was proceeded on several samples deposited at 130°, 150° and 200° without any annealing, deposited at 200° annealed at 450° for 30 minutes and deposited at 130° annealed at 300° and 350° for 15 minutes. The observed morphology was similar in all samples with a nanorods/nanoneedles morphology, as shown in Fig. 18. The estimation of size can confirm the average crystallite size calculated by XRD. It was seen in all samples holes, that were studied by EDX as shown in Figure 19. We can see that inside the hole there is no additional element. With a line studying the distribution of this elements like shown in Figure 19 f), it is possible to observe that inside the hole there is a decrease in Zinc, what suggests that it is just a vacant space where there is no Zinc Oxide. This was most likely caused by the cleaning procedure using acetone and ethanol that left some residues after evaporation, thus leaving a non-deposited zone. Unfortunately, this was noticed quite late and was not possible to re-do all the experiments for having a more uniform deposition. Still this lack of Zinc Oxide will only influence the results, mainly the mobility and conductivity, in a negative way, lowering them, what can suggest that without these holes formation electrical results could be even better.

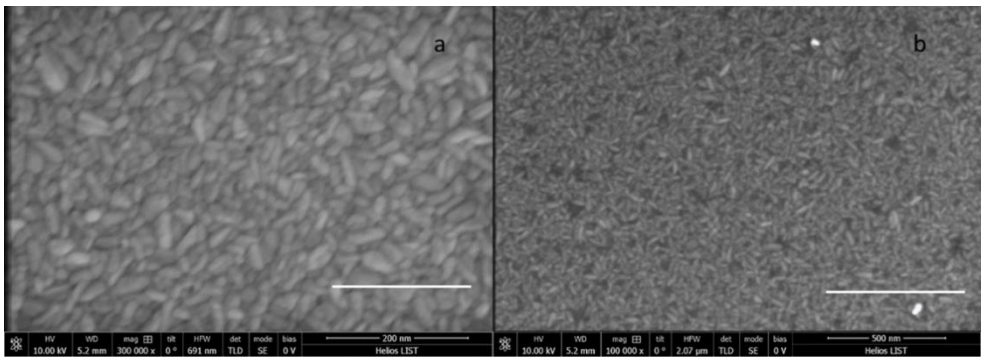

Figure 17 - SEM images of ZnO deposited at 200ºC with a scale of 200nm on a) and 500 nm on b)

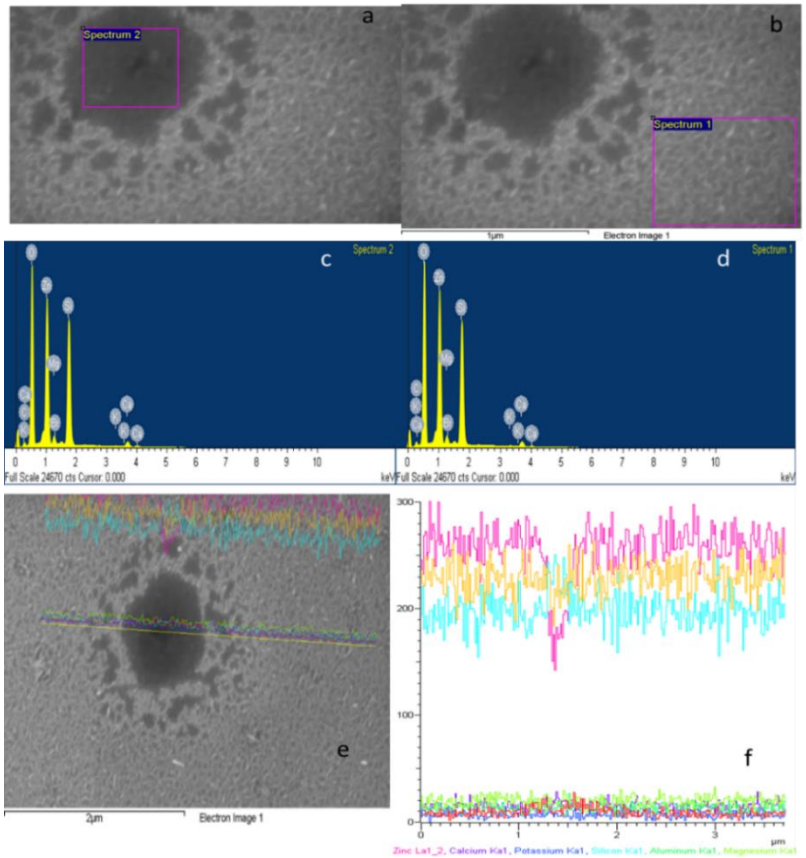

Figure 18 - SEM/EDX imaging and element mapping of ZnO sample deposited at 130°C and annealed at 300° for 15 minutes - a) SEM image with selected spectrum inside the hole; b) SEM image with selected spectrum outside the hole; c) Spectrum of elements inside the hole; d) spectrum of elements outside the hole; e) SEM image of the hole with selected study line; f) Elements in the studied line with great presence of Zn, O and Si

4.1.5 Photoluminescence

Photoluminescence (PL) studies was performed to notice the evolution of the exciton peak of Zinc Oxide thin films with the carrier concentration and potential appearance/disappearance of characteristic peaks related to defects, expected due to the healing of defects with annealing steps. For this it was used two lasers with 325 and 442 nm wavelength. On Figure 20 it is possible to see the spectrum of the PL. Analysing the UV zone in more detail in Figure 20 a), it is possible to see a small shift occurring from the different samples, that if we compare with the carrier concentration is noticeable the red shift with the decrease in carrier concentration, or increase in annealing temperature and annealing time. For the samples deposited at low temperature it is even more visible and is noticeable the decrease in the peak maximum. These conclusions match some literature works such as Wang et al.[26], and Liu et al.[59], This study suggests a decrease of the energy of the excitonic peak that can be related to the optical bandgap with the decrease in carrier concentration at room temperature, what can show the interplay of the electrical and optical properties in Zinc Oxide.

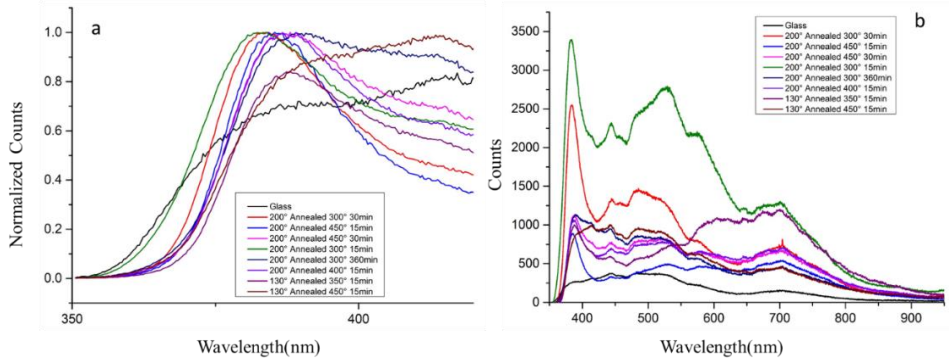

Figure 19 - PL Spectrum with 325nm laser on ZnO thin films: a) Normalized [0, 1] in the UV region; b) original spectrum

The blue laser could give an important information about the defects peak but, due to the deposition of the samples being carried on glass, peaks originating from the substrate are overlapping with the expected ones for the defects. We could thus not analyse the evolution of the peaks related to the defects with annealing steps.

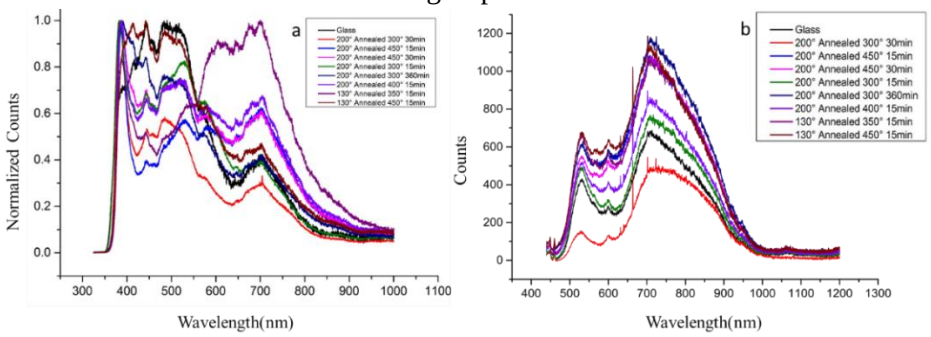

Figure 20- PL spectrum of ZnO thin films: a) with 235nm laser all spectrum normalized; b) with 422nm laser

4.1.6 Conclusion

As a conclusion for the ZnO deposition and annealing for the tunability of the carrier concentration and mobility, it is possible to observe a tunability of the films for a wide range of carrier concentration. Increasing deposition temperature has shown an increase in carrier concentration and in mobility. For the annealing, it was observed a negligible effect of the atmosphere, that can be justified from the fact that both gases used are inert and there is no insertion of dopants but instead only the reorganization and healing of intrinsic point defects. It was noticed the big impact with the temperature and a smaller impact in the annealing time. This can be justified with the fact that the selected times were higher than the relaxation time, what in the logarithmic decrease expected for an activated behaviour means that the influence of a further increase in time will have a rather small effect. Most likely in this case the smallest annealing time used, 900 seconds is already much larger than the relaxation time. Increasing the annealing temperature increases the resistivity, which can be associated with a decrease in carrier concentration and mobility. The observed decrease of the carrier concentration with annealing is always associated with a decrease of the mobility as shown in Figure 13. These interplay is present from carrier concentration of $10^{18}\ cm^{-3}$ to $3 * 10^{19}\ cm^{-3}$, where we find a scaling law with the mobility proportional to the carrier concentration. We attribute this linear dependence to the fact that the scattering mechanism never changes and the number of grain boundaries are kept constant, which was confirmed by XRD and by SEM. Above this carrier concentration seems to be another regime, where the carrier concentration increase is stable in terms of mobility. For AZO samples, it was shown a bigger carrier concentration, above

$10^{21}\ cm^{-3}$, and it was verified a new decrease in mobility with an increase in carrier concentration. The PL analysis show a red shift with decreasing carrier concentration but failed to show a tendency of the defects peaks with changing annealing conditions due to the substrate overlapping its expected peaks.

This work shows that, in order to keep high mobility and try to further decrease carrier concentration, other solutions need to be found, such as changing the deposition parameters.

4.2 CuCrO2

Delafossite films deposited by MOCVD were studied with two kinds of annealing steps, varying the temperature from 650ºC to 850ºC for a fixed time, 15 minutes and keeping the temperature constant at 900ºC and changing the time from 1 to 4000 seconds. It was measured the Seebeck coefficient to make possible the extraction of the carrier concentration using small polaron model. The optical transmittance of the films with different annealing temperatures was analysed.

4.2.1 As-deposited electrical properties

Two sets of $CuCrO_2$ were deposited on 2" sapphire wafers by MOCVD, with similar growth conditions and similar electrical properties. The wafer was cut in approximately 1x1cm squares and in every sample, was measured the conductivity, by four-point-probe and Seebeck coefficient.

Table 4 - As-deposited electrical characteristics of $CuCrO_2$ thin films with error bars from statistical analysis of 12 samples

	Conductivity $(\frac{S}{cm})$	*Seebeck Coefficient* $(\frac{\mu K}{V})$	*Carrier Concentration* cm^{-3}
$CuCrO_2$ As-Deposited	20 ± 8.2	104 ± 7	$1.6 * 10^{21} \pm 2 * 10^{20}$

The sample's thickness was measured by SEM cross-section with values of $200 \pm 40\ nm$. It is to notice that this process still lacks homogeneity in the same wafer there are still very noticeable differences. The Seebeck Coefficient values were negative as expected confirming the p-type behaviour of the films. Hall mobility measurements were not possible in this material, since the mobility was too low, so as an alternative carrier concentration was estimated from the Seebeck Coefficient. The small polaron model was used based on previous literature and works realized by the group[28,29]. Using equation 9, where the density of copper sites in stoichiometric $CuCrO_2$ considering the theoretical lattice is $2.3 * 10^{22}$, and S is the Seebeck coefficient, considering the main mechanism of conduction as being the Cu^{+}/Cu^{2+} [60]. The calculated as deposited mobility was 0.08 cm^2/Vs.

$$p = \frac{1}{1+4\exp\left(S*\frac{e}{Kb}\right)} * 2.3 * 10^{22} \quad \text{(equation 9)}$$

4.2.2 Annealing processes, influence of Temperature and Time

The $CuCrO_2$ presents a very high carrier concentration as-deposited although it has no intentional doping. A further annealing step was required in order to study the possibility to tune the films carrier concentration. It was studied the influence of temperature from 650 to 850°C, keeping the time constant at 15 minutes. The temperature range was chosen following previous work of Gotzendorfer et al.[37] showing that a measurable difference in electrical characteristics of delafossite films is observed only above 620°C. This high temperature might be due to a related activation energy associated with the healing of defects. The influence of time was

studied at a constant temperature 900ºC, and with times ranging from 1 to 4000 seconds. Temperatures above 900ºC were not studied to keep safely bellow the stability limit of Copper delafossite materials that are pointed by previous works to be 1100ºC [60].

For the sample annealed at 900ºC for 4000 seconds, it was not possible to measure the conductivity and the Seebeck coefficient given the instruments range. The Seebeck values annealing annealing prove the p-type conductivity of every film as shown in annex 4. The increasing temperature as well as the increasing time show a major decrease in the film carrier concentration with a film tunability from $10^{21} - 10^{17} cm^{-3}$, over 4 orders of magnitude. The increasing temperature shows a slow decrease in the carrier concentration and more controllable, but for industry processes flash annealing steps at 900°C can be an important solution. In Figure 23 c) and d) the mobility decrease is obvious with any annealing, but a phenomenon occurs in both cases, that after a big decrease, at 700°C and with 30 seconds, the increasing annealing temperature and time does not further decrease the mobility, but instead there is a small recovery. This can prove to be of major importance since the film mobility is rather low and further decreases might prevent to achieve a minor carrier concentration suitable for the electronics applications. Opposite to temperature that the increase in the temperature always cause a bigger decrease in the carrier concentration, in case of time a further increase of time after 200 seconds seems to cause a very small decrease in carrier concentration. This can be explained by the fact that 200 seconds is already larger than the typical relaxation time, and can suggest that this time will be enough for healing of most defects at a given temperature. A further time study with more intermediate points should be done, in order to see the evolution behaviour between 2 and 200 seconds.

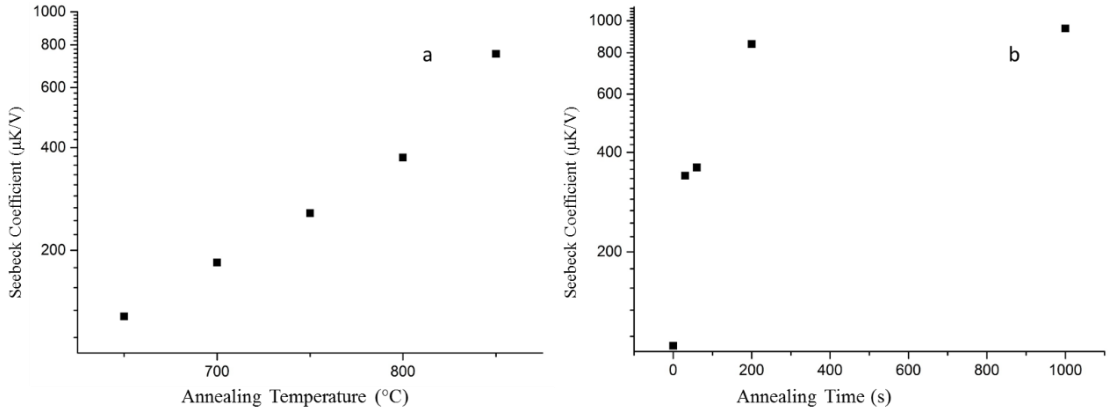

Figure 21 - Seebeck Coefficient of $CuCrO_s$ samples variation with annealing - a) Temperature; b) Time

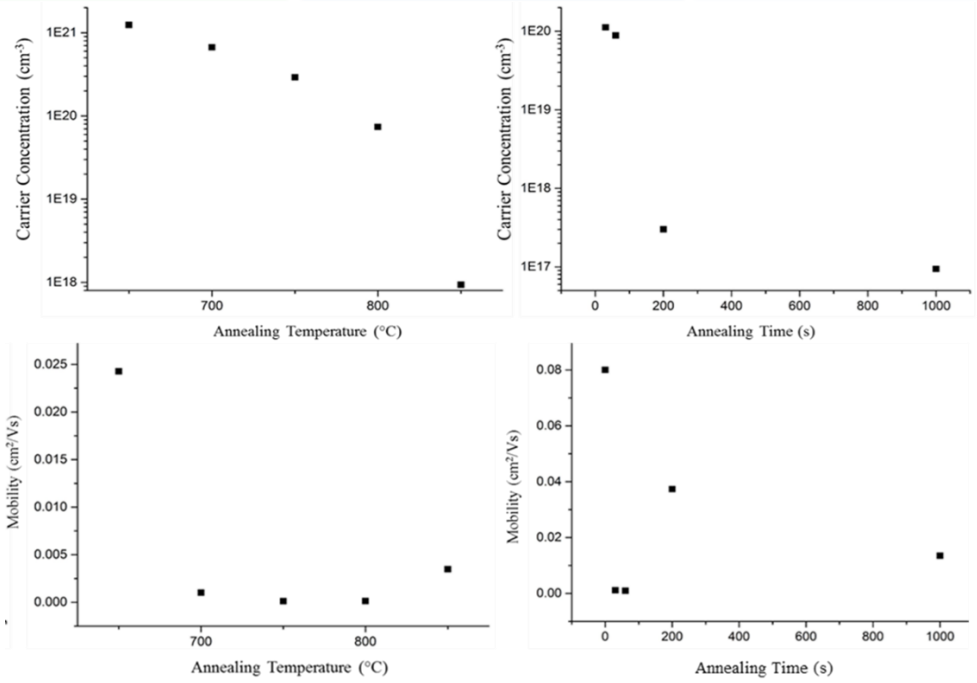

Figure 22- Electrical Properties of $CuCrO_2$ extrapolated using small polaron model variating with annealing conditions: a) Carrier concentration as function of annealing temperature; b) Carrier concentration as function of annealing time; c) Mobility as function of annealing temperature; d) Mobility as function of annealing time

With the considerations made for the annealing time and temperature study, a model was proposed that could explain the carrier concentration behaviour of the films with different annealing steps. The assumed model was the same as the one proposed for the ZnO (see section 4.1.2), reminded in equation 10.

$$\ln(\ln N_0 - \ln p(T,t)) = \ln(At) - \frac{E_a}{k_B T} \qquad \text{equation 10}$$

The calculated time constant at 900ºC, was $k = 0.040 \pm 0.005$ s^{-1}. Taking the "as deposited" carrier concentration as initial dopant concentration $N_0 = 1.6 * 10^{21}$ cm^{-3}, we can plot $\ln(\ln N_0 - \ln p(T,t))$ at fixed annealing time t = 900 s as a function of $1/T$.

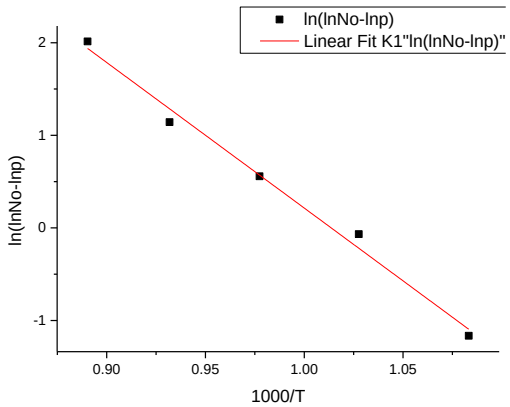

Figure 23 - Linear fit of ln(ln(N0)-ln(p)) vs 1000/annealing Temperature with CuCrO2 annealed at different temperature for a fixed time, 900s

The data fit well with the activation energy model, and we obtain $E_a/k_B = 15700 \pm 900$ K, $E_a = 1.35 \pm 0.07$ eV and $\ln(At) = 15.9 \pm 0.9$ (t = 900 s, A = $8.9 * 10^3$ s^{-1}).

Comparing with the results for the ZnO, we observe a much larger activation energy for healing of defects in $CuCrO_2$, what is agreeing with the fact that the delafossite films require much higher temperature to have a similar decrease in carrier concentration for the same time.

Table 5 - Bibliography values for defect healing and diffusion

Ref.	Material	Defect	Ea (eV)	Comment
Allen [61]	GaAs	V_{Cr}	0.8	V_{cr} Defect Healing
Karoui et al. [62]	Si	O_i	2.5	Diffusion of O_i
Needels et al.[63]	Si	O_i	1.8	Theory Value PBE
Biccari [64]	Cu_2O	V_{Cu}	0.55	Diffusion energy

4.2.3 Optical Properties

The optical properties of the $CuCrO_2$ were studied to see the applicability of this films in a transparent junction, it would be important to have a major transmittance in the visible region. It was visible an increase in the optical transmittance of the samples with the increased annealing time and temperature, except for the sample annealed at 650°C. Still from as-deposited to the sample annealed for 1000s at 900°C there is a major increase in transmittance values from 38% to 60% in the optical range, what is quite good for transparent electronics since it requires an annealing step, due to the high carrier concentration of the films as deposited, and the maximum transmittance in the visible range possible. The optical results would be enhanced using another substrate since the sapphire has optical transmittances around 80%. Still a glass substrate would not be possible due to the high temperature annealing temperature processes.

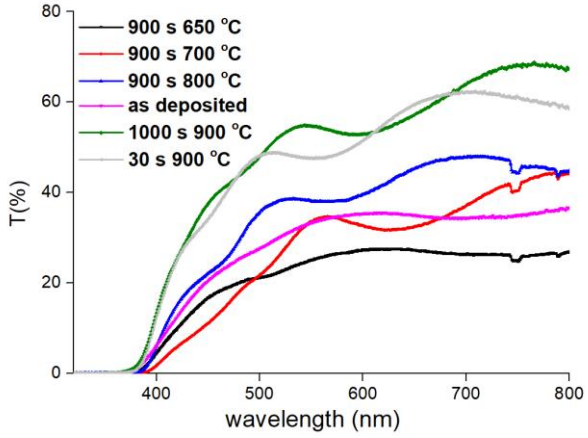

Figure 24 - CuCrO2 films transmittance in the visible range, samples annealed under different conditions

4.2.4 Conclusion

$CuCrO_2$ samples deposited at 450ºC presented a quite high carrier concentration, $1.6 * 10^{21}\ cm^{-3}$. The two annealing routes proposed showed different behaviours. With increasing temperature, the decrease in carrier concentration was controllable with a bigger precision tunability, while the variation of time showed a clear logarithmic behaviour with a quick decrease up to 200 seconds and then a tendency to a residual doping concentration. With this a model was proposed that related carrier concentration with temperature and time. It was retrieved an activation energy, E_a = 1.35 ± 0.07 eV. This energy is expected to be related to healing of the missing Cu lines, proposed to be the defect mechanism in the group deposited $CuCrO_2$ [60]. The required annealing step if favoured also by the increase of the optical transmittance of the films.

4.3 P-N Junction

As a result of the study of these materials we developed a p-n junction that could be a promising building block for the transparent microelectronics. It was studied the band alignment of the materials projected from the literature and from a simulation software. KPFM studies were performed on ZnO and $CuCrO_2$ films in order to compare the evolution of the Fermi level with the carrier concentration and so study the band alignment type in all cases. $CuCrO_2$ films were deposited on a sapphire wafer and annealed. On top was deposited ZnO that was also annealed and further patterned by photolithography and etching. Lastly it was made I-V traces of the potential junction.

4.3.1 Simulation of the p-n junction

The simulation was used to predict the band alignment and the appropriate carrier concentration to be proposed for the junction. These values were compared with the literature.

According to literature the best results for a P-N junction with similar materials to the used ones in order to maximize the rectification factor and the ideality factor and to have a good band alignment would be having a junction with doping in both sides in the range of $10^{17} - 5 * 10^{19}\ cm^{-3}$. These junctions have achieved values On/Off ratio of 86 [66], with a both sides carrier concentration of $5 * 10^{18}\ cm^{-3}$. A band diagram is represented in Figure 26, where it is possible to verify the type-II band-alignment predicted for a junction with these materials.

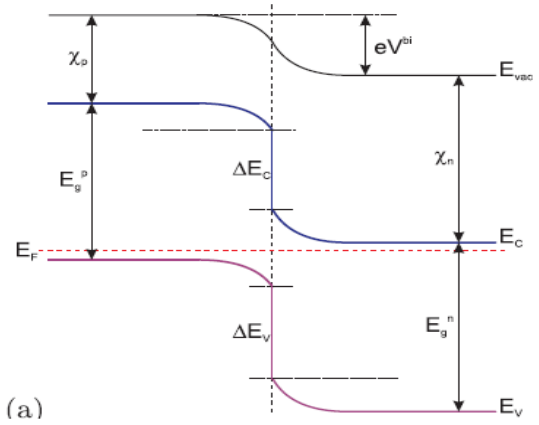

Figure 25 - Type-II band alignment schematic adapted from Grundmann et al.[49]

The expected junction was simulated using a 1D Poisson-Schrödinger solver (developed by Greg Snider), where we introduced the two new materials, $CuCrO_2$ and ZnO. The software can provide an interesting first preview of the band alignment and it is also possible to predict a doping profile and so extract the depletion region. A more detailed report can be found on annex 4. Still from the software it was possible to extract that a carrier concentration of at least $10^{18}\ cm^{-3}$ should be necessary for having an Off-State at 0V bias and that $10^{20}\ cm^{-3}$ could induce a too small depletion region for the junction, that could permit electron tunneling. From the junction, it is supposed that any carrier concentration in between $10^{18}\ cm^{-3}$ and $10^{19}\ cm^{-3}$ can work, showing a type-II band alignment, as shown in Figure 27, with a P-N junction using a carrier concentration on both sides of $5 * 10^{18}\ \mathrm{cm}^{-3}$, that matches the predicted band alignment and that can potentialize the junction and was shown also that junctions with different carrier concentration profiles can work, mostly well if the more doped side is P-type.

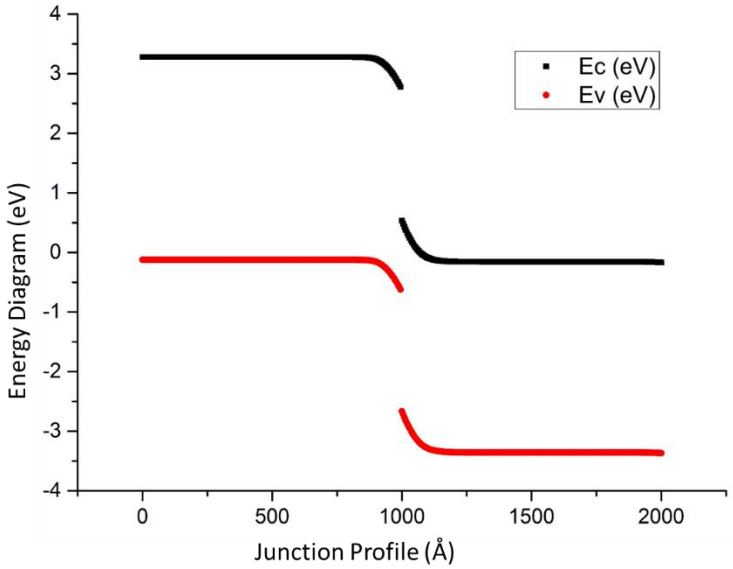

Figure 26- Junction Simulation with carrier concentration on both sides of $5 * 10^{18}\ cm^{-3}$

4.3.2 KPFM Results

KPFM was performed on both ZnO and $CuCrO_2$ samples. The KPFM results can give an important information about the Fermi level movement and so predict the different band-alignment for the junction with the different doping levels.

For ZnO samples it was performed on sample 9 (Deposited at 200°C annealed at 450° for 60 minutes) and on sample 1 (Deposited at 200° Annealed at 300°C 15 min). The KPFM analysis was made always in comparison with a HOPG sample that has a well-defined work function. This permitted minimize contamination interference since the measurement was always made one at a time between graphene and the desired sample. The results presented on Figure 29 and 30 are following Difference to HOPG = ΦSample-ΦHOPG$(4{,}6eV)$, what means that if Fermi level increases, the Φ of the sample will decrease and the difference to HOPG will decrease too because the HOPG workfunction is constant. The mapping produced by the KPFM measurement is shown in Figure 28 and with the histogram produced by this mapping the peak is used as the effective workfunction difference value. In Figure 29 it is shown that the decrease in carrier concentration, with increased annealing temperature and time shows a positive increasing to HOPG, what confirms a shift of the Fermi level from near the conduction band to a lower energy.

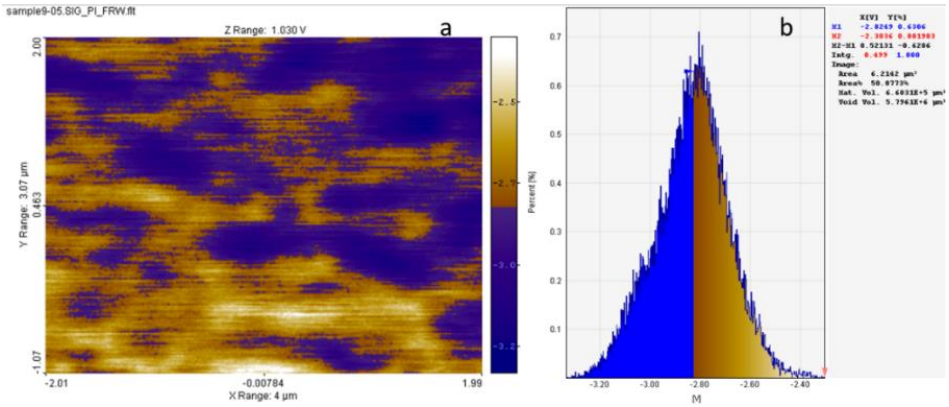

Figure 27 - a) Mapping of surface potential performed by KPFM measurement on ZnO sample '9'; b) Histogram associated with the map of a)

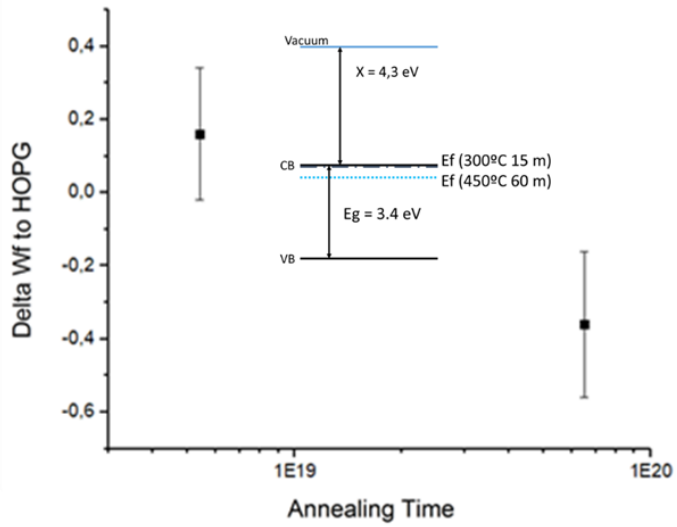

Figure 28 - Evolution of Difference to HOPG measurements produced by KPFM vs Carrier Concentration of ZnO samples '1' and '9, with an inset energy diagram of the variable position of the Fermi level with different annealing conditions

In Figure 29, is presented the two analysed ZnO samples with a schematic of the position of the relative Fermi level in the band diagram, with two different annealing conditions, deposited at the same temperature, 200ºC. The considered electron affinity of ZnO was 4.3eV from Tharsika et al. work [67]. The presented error bars are from the width at half peak of the histogram.

In the case of the $CuCrO_2$ films exactly the opposite behaviour is expected with the increase in workfunction with the increase in carrier concentration, this is confirmed by the tests made, represented in Figure 30. In this Figure, there is a schematic that projects the different Fermi level depending on the annealing conditions using as reference values for electron affinity from Wang et al.[68], that estimated it to be 2.1eV for the $CuCrO_2$ and the bandgap to be 3.2eV. On the right side of this axis it is represented the shift of the Fermi level compared to the maximum of the valence band projected for this delafossite, equation 11.

$$Ef - Ev = (X + Eg) - \Delta Wf \quad \text{(equation 11)}$$

Billard et al.[45], present for their high carrier concentration thin films that the workfunction is 5.01eV, what can be fitting to the projected carrier concentration in Figure 30 – b) with a carrier concentration of approximately $10^{21} cm^{-3}$.

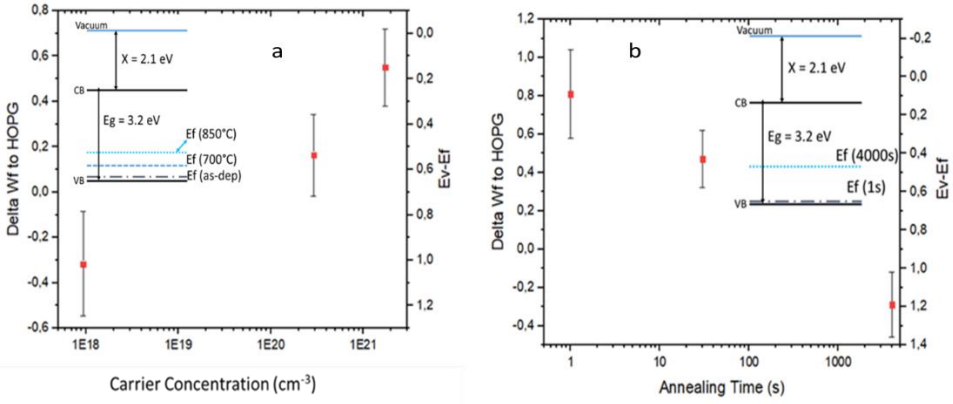

Figure 29 - CuCrO2 samples Workfunction difference to HOPG as function of: a) Annealing Time; b) Carrier Concentration; with an inset energy diagram of the variable position of the Fermi level with different annealing conditions

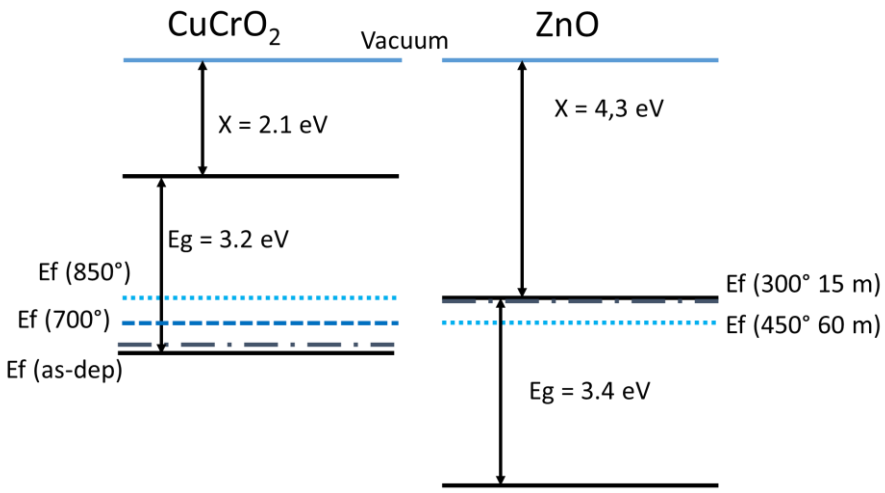

Figure 30 - Schematic of the band alignment, showing the type-II alignment with the different Fermi levels depending on the annealing conditions

Figure 31 shows the predicted band-alignment with the values retrieved from the literature and the predicted Fermi levels from the KPFM analysis. It is shown that a possibly good rectification can occur when the $CuCrO_2$ is annealed at 850ºC and ZnO is annealed at 450ºC. For instance, it is also possible to see if the $CuCrO_2$ is annealed for 700ºC the Fermi levels are aligned, and no depletion layer is expected in this case.

4.3.3 Junction Development

For the final device, we used 3 samples with $CuCrO_2$ deposited using the same conditions on a sapphire wafer. They were cut in 3 squares of 1x1cm. The conductivity of these samples was slightly higher than the ones investigated in section 4.2, for the annealing of CuCrO2. They were annealed at different temperatures for trying to compare the different carrier concentration influence on the rectification factor of the junction.

Table 6 - CuCrO2 thin films as deposited and annealed used for the junction - electrical characteristics, for samples as deposited error is extracted from statistical analysis of the three samples, for the others the Seebeck coefficient error is extracted from the fitting

	Conductivity $(\frac{S}{cm})$	*Seebeck Coefficient* $(\frac{\mu K}{V})$	*Carrier Concentration* cm^{-3}
$CuCrO_2$ As-Deposited	30 ± 6	-80 ± 2	$2.1 * 10^{21} \pm 2 * 10^{20}$
1 -Annealed at 850°C for 5 minutes	$8 * 10^{-4}$	-380 ± 27	$7 * 10^{19}$
2 - Annealed at 800°C for 30 minutes	$3.8 * 10^{-3}$	-410 ± 18	$5 * 10^{19}$
3 - Annealed at 900°C for 1 minute	$2.7 * 10^{-2}$	-240 ± 4	$3.5 * 10^{20}$

The samples used for the junction presented a higher carrier concentration as-deposited and so, the programmed annealing processes didn't decrease the carrier concentration as much as expected. Still it was tried to process the junction with these high carrier concentrations.

On top of the CuCrO2 film, we have deposited a ZnO film at 150ºC, with a thickness of 65nm. The different junction samples were annealed through different steps, in N_2 atmosphere with sample 3 being annealed for 15 min at 150ºC and sample 2 at 200ºC for 5 min prior to etching, and sample 1 was annealed after the etching. The electrical results, measured on samples deposited on the same ALD process and in the same annealing chamber, are shown in Table 7.

Table 7 - ZnO thin films as deposited and annealed deposited on top of $CuCrO_2$ - electrical characteristics

	Conductivity ($\frac{S}{cm}$)	*Mobility*(cm^2/Vs)	*Carrier Concentration* (cm^{-3})
ZnO As-Deposited	55.8 ± 3	9.3 ± 1	$3.5 * 10^{21} \pm 3 * 10^{20}$
1/3 - Annealed at 150°C for 15 minutes	11.9	7.2	$8 * 10^{18}$
2 - Annealed at 200°C for 5 minutes	14.1	4.9	$1.7 * 10^{19}$

The bi-layer was further patterned to give nine junctions in each of the samples, three of each of the chosen sizes, 250, 500 and 1000 µm.

4.3.3.1 Etching

Etching process was studied for patterning ZnO for the junction with the objective of creating several pads of ZnO. Ideally an anisotropic etching would enable further miniaturization so it was studied the reactive ion etching process with the available gases, CF_4 and Ar on a 80-20% ratio, with 500W RF power. The resulting etching rate was 0.14 nm/sec. However, the bilayer photoresist used for the lithography step was completely etched and the silicon beneath was also partially etched. So, a wet etching process was preferred. It was used a $FeCl_2$ solution at 0.1%, that had previously been found to have an etching rate of 6 nm/s. In Figure 32 is represented a SEM image of a ZnO sample on Silicon substrate, 135 nm thick with an undercut of 124 nm. This wet etching process is highly isotropic presenting almost a ratio 1:1 in lateral and vertical etching.

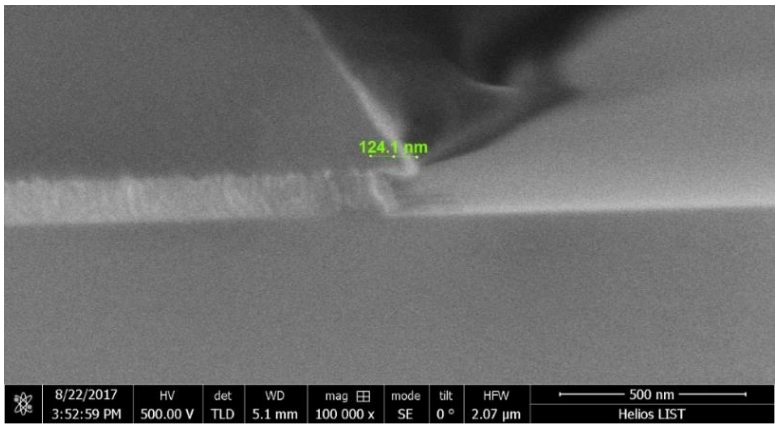

Figure 31 - ZnO Film with 135 nm covered with photoresist etched in $FeCl_2$ for 20 seconds, presenting an undercut of 124 nm.

All the etchings were processed with $FeCl_2$ for 15 seconds, what should give a total etching of 90 nm to have a safe margin. During the etching process of sample 3, the ZnO layer was removed completely, leaving the electrical analysis of the junction to sample 1 and 2. Optical images showing the junction are present in annex 5.

4.3.4 Device Characterization

The electrical characterization with I-V curves presented a ohmic behaviour. Unfortunately, this behaviour was presented in every pad, instead of the expected rectification behaviour. In order to reduce the contact resistance to the CuCrO2 layer, silver paste was used on this layer, still giving ohmic behaviour of the junction, as shown in Figure 33-a). Equivalent results were presented in both sample 1 and sample 2. There are several factors that can impact these measurement, the fact that there is no barrier and the materials behave like a contact is most likely due to too high carrier concentration.

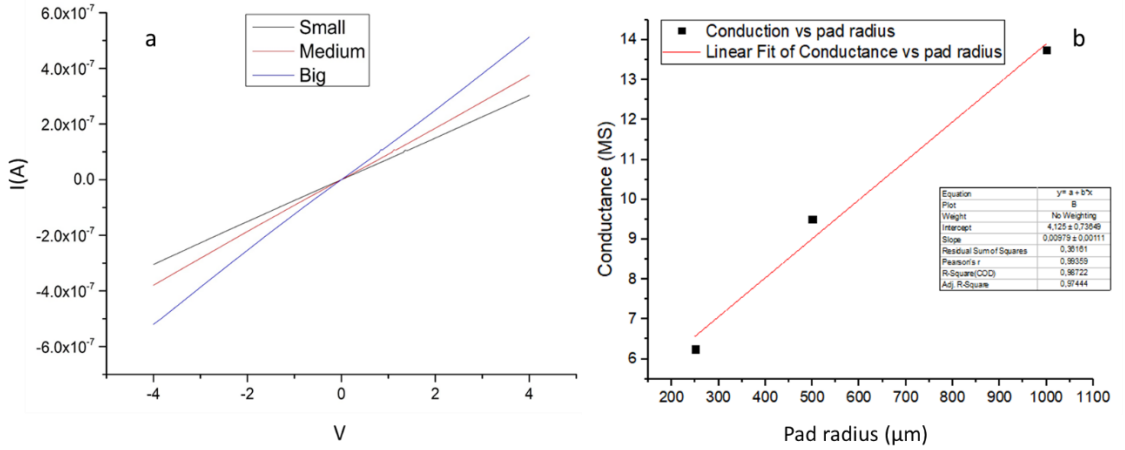

Figure 32 – a) I-V Curves of different pads in sample 2 with a sweep from -4 to 4 V; b) Conductance (slope from I-V curves) vs pad radius showing the contact size dependence

The fact that there are no contacts on bottom and top can also play an important role in increasing the series resistance. It was checked if all the ZnO had been removed through EDX as shown in Figure 36 and was made top imaging of the junction, image 34 and 35. The ZnO is completely removed as we can see in the EDX and the junction presents a clear distinction between the $CuCrO_2$ on the right and the ZnO grains on the left. This points that the junction was well processed, the etching worked quite well, but still the carrier concentration was not the most adequate and should have been made longer/higher temperature annealing to try to tune the carrier concentration to values close to $5 * 10^{18} cm^{-3}$.

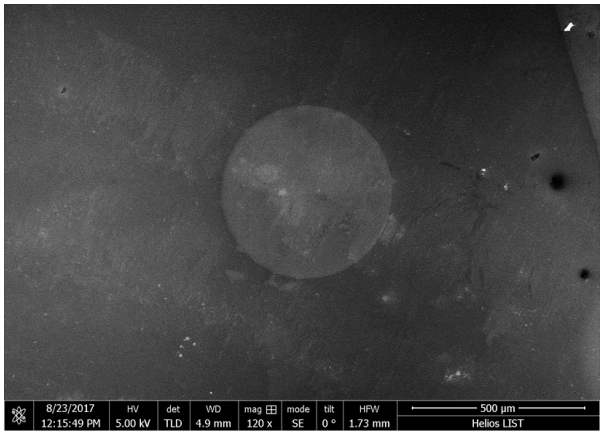

Figure 33- SEM image of the junction with a ZnO pad with 250µm radius

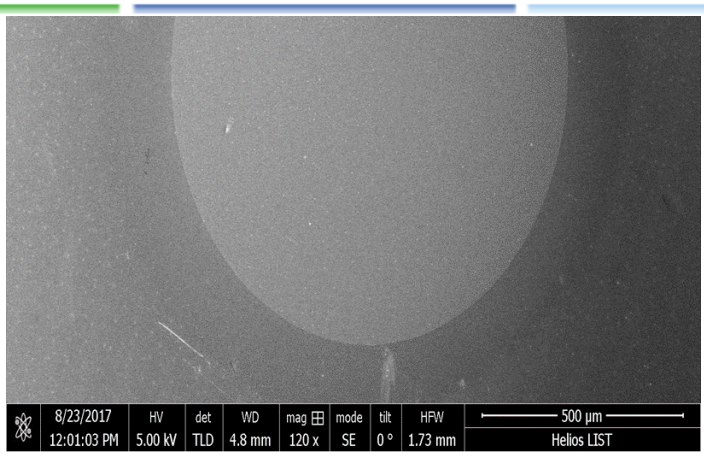

Figure 34 - SEM image of the junction with a ZnO pad with 500µm radius

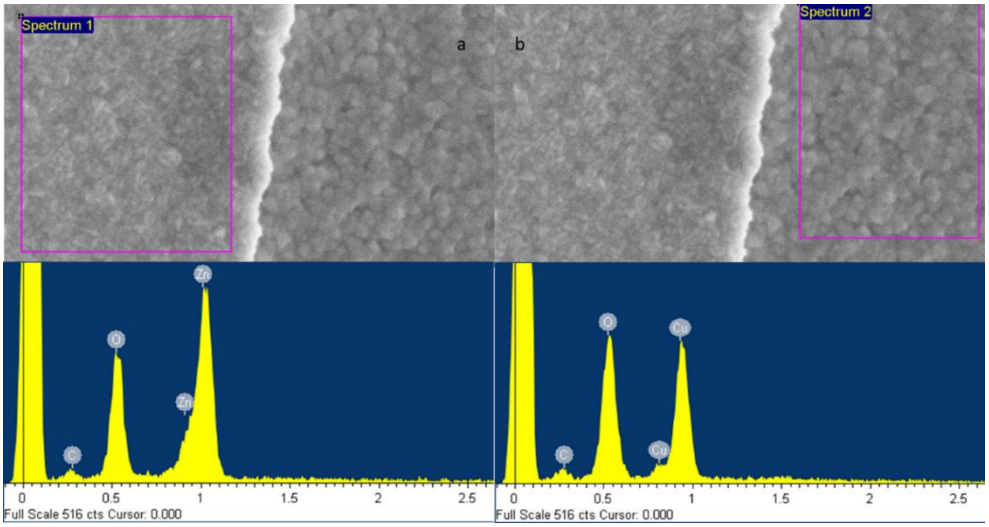

Figure 35- SEM image of the junction with the elements present on each side of the junction, with a) ZnO b) $CuCrO_2$

5 Conclusion and Future Perspectives

In this work ZnO films were deposited by ALD in temperatures ranging from 130º to 200ºC. They were further annealed for carrier concentration and mobility control studies. MOCVD deposited $CuCrO_2$ films was also studied for transparent electronics applications. A P-N junction was built and characterized.

The annealing of the $CuCrO_2$ proposed by the two methods, changing the temperature with a fixed time (15 minutes) and changing time, with fast annealing steps at high temperature (900ºC), englobe a wide range of tunability of the films that can in the first case have a wide variation smoothly due to the lower temperatures and in the second case can be very important to match the fast processes required by the industries for devices such as junctions or transistors, keeping the process safely bellow the temperature of stability limit (1100ºC). Annealing of $CuCrO_2$ has shown a tunability in terms of carrier concentration from $2 * 10^{21}$ approaching $10^{17} cm^{-3}$, a over four orders of magnitude change. An associated activation energy with the defects healing was calculated to be 1.35eV, with the relaxation and thermal activated model proposed. An important conclusion retrieved from this annealing step was the increase in optical transmittance in the films with the increasing annealing temperature, so the annealing step permitted not only to adjust the film carrier concentration, to be more suitable for microelectronics applications as it increased the transmittance in the optical region. The ability to manipulate the Fermi level shown by KPFM can prove of great importance in tailoring of such devices. The $CuCrO_2$ films keep showing an exciting potential, still without the high mobility presented by the n-type films, that probably will never be achieved, but with the capacity to still present good conductivities.

The ZnO films confirmed the projected wide range of applications they are suggested for, capable of being tuned for an immense carrier concentration, even more if we include AZO films that can be a very good transparent contact. Different deposition temperatures were studied, showing an increase in the carrier concentration and mobility with the increase in deposition temperature. Annealing studies were performed under different atmosphere, time and temperatures. The inert atmospheres used, Ar and N_2 have shown no difference between them. The time influence was rather small, because of the minimum time used was larger than the relaxation time. So in this case the main influence was driven by the annealing temperature. With the model proposed the activation energy for defects healing was calculated to be 0.31eV. The study of the ZnO films permitted to conclude that even though it is possible to have a great tunability of the films there seems to be an associated decrease in the mobility with the decrease in carrier concentration for values bellow $3 * 10^{19} cm^{-3}$, that can not be surpassed, this was confirmed with further XRD and SEM analysis that show that there seems not to be a decrease in the grain size that could increase the number of grain boundaries and be responsible for the decrease in mobility. In SEM analysis, there appears to be a flaw in this work that show the films with vacant spots of Zinc Oxide, possibly due to the cleaning with acetone before the deposition. The PL the patterning was processed using wet etching, with a $FeCl_2$ 0.1% solution combined with photolithography. The final device was tested with three different radii to analyse the influence of the area on the device. Unfortunately, the final junction did not work properly and presented no rectification factor but a ohmic behaviour, what can be explained by the real carrier concentrations used in the junction comparing with the KPFM studied before, that predicted that to have a rectification factor instead of the contact behaviour it would be needed to have a much lower carrier concentration, about $5 * 10^{18} cm^{-3}$, than the one used.

The junction proposed in this work, was never achieved due to delays in the delivery of sapphire with Fluorine Tin Oxide (FTO) deposited on top. For so it was not possible to have a

bottom contact that was compatible with the temperature that was required for the $CuCrO_2$ annealing and it was tried a simple junction without contacts on top and bottom and for so a more conductive film was used than the firstly expected.

Still this work explores the wide range of carrier concentration achievable for the films and their potential applications for transparent microelectronics. Although this work comes close, in exploring the materials, in applying these materials to the main building block a P-N junction, with its patterning and execution it is not finished, since the planned junction was not achieved. For this there are still objectives that could be met in the near future, both in the material as studies and junction development, as:

- Further study of the defect healing activation energy with various times and various temperatures for both materials.
- Study the Photoluminescence in another substrate that is not glass in order to compare the defect characteristic peaks with the evolution in carrier concentration and activation energy for each temperature.
- Study ways to further uniformize the $CuCrO_2$ deposition process and have a wider study of its annealing.

- Apply the studied materials into a P-N junction using a lower carrier concentration, as the projected and confirmed by KPFM studies of $5 * 10^{18} cm^{-3}$
- Develop the junction using a bottom contact such as FTO that can stand high temperatures and a top contact such as AZO film in order to decrease the contact resistance of the junction and maximize its electrical properties.

- Study the introduction of these materials in another transparent electronics applications such as CMOS transistors and as solar cells hole transport and electron transport materials, as suggested in Figure 37.

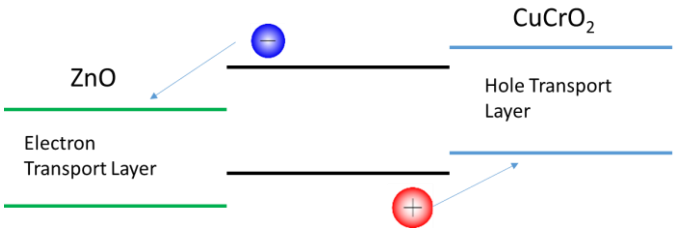

Figure 36- Potential solar cell using ZnO and $CuCrO_2$ as electron transport layer and hole transport layer

6 Bibliography

1. Muchuweni, E., Sathiaraj, T. S. & Nyakotyo, H. Synthesis and characterization of zinc oxide thin films for optoelectronic applications. *Heliyon* **3,** e00285 (2017).
2. Leenheer, A. J. *et al.* General mobility and carrier concentration relationship in transparent amorphous indium zinc oxide films. *Phys. Rev. B* **77,** 115215 (2008).
3. Lee, J.-H., Ko, K.-H. & Park, B.-O. Electrical and optical properties of ZnO transparent conducting films by the sol–gel method. *J. Cryst. Growth* **247,** 119–125 (2003).
4. Laube, J. *et al.* Resistivity of atomic layer deposition grown ZnO: The influence of deposition temperature and post-annealing. *Thin Solid Films* **603,** 377–381 (2016).
5. Banerjee, P., Lee, W.-J., Bae, K.-R., Lee, S. B. & Rubloff, G. W. Structural, electrical, and optical properties of atomic layer deposition Al-doped ZnO films. *J. Appl. Phys.* **108,** 43504 (2010).
6. Dimova-Malinovska, D. Nanostructured ZnO Thin Films: Properties and Applications BT - Nanotechnological Basis for Advanced Sensors. in (eds. Reithmaier, J. P., Paunovic, P., Kulisch, W., Popov, C. & Petkov, P.) 157–166 (Springer Netherlands, 2011). doi:10.1007/978-94-007-0903-4_16
7. Sharma, S., Vyas, S., Periasamy, C. & Chakrabarti, P. Structural and optical characterization of ZnO thin films for optoelectronic device applications by RF sputtering technique. *Superlattices Microstruct.* **75,** 378–389 (2014).
8. O'Brien, S. *et al.* Zinc oxide thin films: Characterization and potential applications. *Thin Solid Films* **518,** 4515–4519 (2010).
9. Özgür, Ü. *et al.* A comprehensive review of ZnO materials and devices. *J. Appl. Phys.* **98,** 1–103 (2005).
10. Pung, S.-Y., Choy, K.-L., Hou, X. & Shan, C. Preferential growth of ZnO thin films by the atomic layer deposition technique. *Nanotechnology* **19,** 435609 (2008).
11. Farley, N. R. S. *et al.* Sol-gel formation of ordered nanostructured doped ZnO films. *J. Mater. Chem.* **14,** 1087–1092 (2004).
12. Wang, Z. L. Nanostructures of zinc oxide. *Mater. Today* **7,** 26–33 (2004).
13. Malm, J., Sahramo, E., Perälä, J., Sajavaara, T. & Karppinen, M. Low-temperature atomic layer deposition of ZnO thin films: Control of crystallinity and orientation. *Thin Solid Films* **519,** 5319–5322 (2011).
14. Iqbal, J. *et al.* ALD grown nanostructured ZnO thin films: Effect of substrate temperature on thickness and energy band gap. *J. King Saud Univ. - Sci.* **28,** 347–354 (2016).
15. Park, H. K. *et al.* Purge-time-dependent growth of ZnO thin films by atomic layer deposition. *J. Alloys Compd.* **605,** 124–130 (2014).
16. Lee, J. H. & Park, B. O. Transparent conducting ZnO:Al, In and Sn thin films deposited by the sol-gel method. *Thin Solid Films* **426,** 94–99 (2003).
17. Lim, S. J., Kwon, S. & Kim, H. ZnO thin films prepared by atomic layer deposition and rf sputtering as an active layer for thin film transistor. *Thin Solid Films* **516,** 1523–1528 (2008).
18. Tynell, T. & Karppinen, M. Atomic layer deposition of ZnO: a review. *Semicond. Sci. Technol.* **29,** 43001 (2014).
19. Illiberi, A., Roozeboom, F. & Poodt, P. Spatial Atomic Layer Deposition of Zinc Oxide Thin Films. *ACS Appl. Mater. Interfaces* **4,** 268–272 (2012).
20. Park, S.-H. K., Hwang, C.-S., Kwack, H.-S., Lee, J.-H. & Chu, H. Y. Characteristics of ZnO Thin Films by Means of Plasma-Enhanced Atomic Layer Deposition. *Electrochem. Solid-State Lett.* **9,** G299–G301 (2006).
21. Huby, N., Ferrari, S., Guziewicz, E., Godlewski, M. & Osinniy, V. Electrical behavior of

zinc oxide layers grown by low temperature atomic layer deposition. *Appl. Phys. Lett.* **92,** 23502 (2008).

22. Maragliano, C. *et al.* Quantifying charge carrier concentration in ZnO thin films by Scanning Kelvin Probe Microscopy. **4,** 4203 (2014).
23. Lin, B., Fu, Z., Jia, Y. & Liao, G. Defect Photoluminescence of Undoping ZnO Films and Its Dependence on Annealing Conditions. *J. Electrochem. Soc.* **148,** G110 (2001).
24. Lim, J., Shin, K., Woo Kim, H. & Lee, C. Photoluminescence Studies of ZnO thin films grown by atomic layer epitaxy. *J. Lumin.* **109,** 181–185 (2004).
25. Geng, Y. *et al.* Effects of Rapid Thermal Annealing on Structural, Luminescent, and Electrical Properties of Al-Doped ZnO Films Grown by Atomic Layer Deposition. *ECS J. Solid State Sci. Technol.* **1,** N45–N48 (2012).
26. Wang, A. *et al.* Effects of doping and annealing on properties of ZnO films grown by atomic layer deposition. *Nanoscale Res. Lett.* **10,** 75 (2015).
27. Liu, Y., Li, Y. & Zeng, H. ZnO-Based Transparent Conductive Thin Films : Doping , Performance , and Processing. **2013,** (2013).
28. Lunca Popa, P., Crêpellière, J., Leturcq, R. & Lenoble, D. Electrical and optical properties of Cu-Cr-O thin films fabricated by chemical vapour deposition. *Thin Solid Films* **612,** 194–201 (2016).
29. Crêpellière, J. *et al.* Transparent conductive CuCrO2 thin films deposited by Pulsed Injection Metal Organic Chemical Vapor Deposition: up-scalable process technology for an improved transparency/conductivity trade-off. *J. Mater. Chem.* 31–37 (2016). doi:10.1039/x0xx00000x
30. Nagarajan, R., Draeseke, A. D., Sleight, A. W. & Tate, J. p-type conductivity in CuCr1-xMgxO2 films and powders. *J. Appl. Phys.* **89,** 8022–8025 (2001).
31. Kawazoe, H. *et al.* P-type electrical conduction in transparent thin films of CuAlO2. *Nature* **389,** 939–942 (1997).
32. Scanlon, D. O. & Watson, G. W. Understanding the p-type defect chemistry of CuCrO2. *J. Mater. Chem.* **21,** 3655 (2011).
33. Marquardt, M. A., Ashmore, N. A. & Cann, D. P. Crystal chemistry and electrical properties of the delafossite structure. *Thin Solid Films* **496,** 146–156 (2006).
34. Kawazoe, H., Yanagi, H., Ueda, K. & Hosono, H. Transparent p-Type Conducting Oxides: Design and Fabrication of p-n Heterojunctions. *MRS Bull.* **25,** 28–36 (2000).
35. Ingram, B. J. *et al.* Transport and Defect Mechanisms in Cuprous Delafossites. 1. Comparison of Hydrothermal and Standard Solid-State Synthesis in CuAlO2. *Chem. Mater.* **16,** 5616–5622 (2004).
36. Nagarajan, R. *et al.* p-Type conductivity in the delafossite structure. *Int. J. Inorg. Mater.* **3,** 265–270 (2001).
37. Götzendörfer, S., Polenzky, C., Ulrich, S. & Löbmann, P. Preparation of CuAlO2 and CuCrO2 thin films by sol-gel processing. *Thin Solid Films* **518,** 1153–1156 (2009).
38. Neumann-Spallart, E. C. and M. B. and M. G. and T. T. and D. D. and D. J. and A. S. and Y. D. and M. Control of p-type conduction in Mg doped monophase CuCrO 2 thin layers. *J. Phys. D. Appl. Phys.* **49,** 205107 (2016).
39. Arnold, T. *et al.* X-ray spectroscopic study of the electronic structure of CuCrO2. *Phys. Rev. B - Condens. Matter Mater. Phys.* **79,** 1–9 (2009).
40. Scanlon, D. O., Godinho, K. G., Morgan, B. J. & Watson, G. W. Understanding conductivity anomalies in CuI-based delafossite transparent conducting oxides: Theoretical insights. *J. Chem. Phys.* **132,** 24707 (2010).
41. Cusco, C. D. *et al.* Transport and Defect Mechanisms in Transport and Defect Mechanisms in Cuprous. *Chem. Mater.* **79,** 5623–5629 (2004).
42. Barnabe, A., Thimont, Y., Lalanne, M., Presmanes, L. & Tailhades, P. p-Type

conducting transparent characteristics of delafossite Mg-doped CuCrO2 thin films prepared by RF-sputtering. *J. Mater. Chem. C* **3,** 6012–6024 (2015).

43. Benreguia, N., Barnabé, A. & Trari, M. Sol--gel synthesis and characterization of the delafossite CuAlO2. *J. Sol-Gel Sci. Technol.* **75,** 670–679 (2015).
44. Li, S. Z. *et al.* Epitaxial growth of delafossite CuFeO2 thin films by pulse laser deposition. *Phys. B Condens. Matter* **407,** 2412–2415 (2012).
45. Billard, H. S. and M. A. P. Y. and F. S. and A. Optoelectronic properties of delafossite structure CuCr 0.93 Mg 0.07 O 2 sputter deposited coatings. *J. Phys. D. Appl. Phys.* **49,** 185105 (2016).
46. Rastogi, A. C., Lim, S. H. & Desu, S. B. Structure and optoelectronic properties of spray deposited Mg doped p-CuCrO2 semiconductor oxide thin films. *J. Appl. Phys.* **104,** 23712 (2008).
47. Cheng, Y.-C., Yuan, K.-Y. & Chen, M.-J. ZnO thin films prepared by atomic layer deposition at various temperatures from 100 to 180 °C with three-pulsed precursors in every growth cycle. *J. Alloys Compd.* **685,** 391–394 (2016).
48. Lim, J., Shin, K., Kim, H. W. & Lee, C. Effect of annealing on the photoluminescence characteristics of ZnO thin films grown on the sapphire substrate by atomic layer epitaxy. *Mater. Sci. Eng. B* **107,** 301–304 (2004).
49. Grundmann, M. *et al.* Oxide bipolar electronics: materials, devices and circuits. *J. Phys. D. Appl. Phys.* **49,** 213001 (2016).
50. Ye, Y. *et al.* 4.2: *Invited Paper* : Development of High Mobility Zinc Oxynitride Thin Film Transistors. *SID Symp. Dig. Tech. Pap.* **44,** 14–17 (2013).
51. Jin, J. D. *et al.* Tuning the electrical properties of ZnO thin-film transistors by thermal annealing in different gases. *Thin Solid Films* (2014). doi:10.1016/j.tsf.2013.12.004
52. Minami, T., Suzuki, S. & Miyata, T. Electrical Conduction Mechanism of Highly Transparent and Conductive ZnO Thin Films. *Mater. Res.* **666,** 1–7 (2001).
53. Kennedy, J., Murmu, P. P., Leveneur, J., Markwitz, A. & Futter, J. Applied Surface Science Controlling preferred orientation and electrical conductivity of zinc oxide thin films by post growth annealing treatment. *Appl. Surf. Sci.* **367,** 52–58 (2016).
54. Lu, L. & Wong, M. The resistivity of zinc oxide under different annealing configurations and its impact on the leakage characteristics of zinc oxide thin-film transistors. *IEEE Trans. Electron Devices* **61,** 1077–1084 (2014).
55. Ke, L., Lai, S. C., Ye, J. D., Kaixin, V. L. & Chua, S. J. Point defects analysis of zinc oxide thin films annealed at different temperatures with photoluminescence , Hall mobility , and low frequency noise Point defects analysis of zinc oxide thin films annealed at different temperatures with photoluminescence ,. **84502,** (2012).
56. Golshahi, S., Rozati, S. M. & Ghasempoor, T. ANNEALING TREATMENT OF ZnO THIN FILMS PREPARED BY NON- REACTIVE E-BEAM EVAPORATION TECHNIQUE. *Dig. J. Nanomater. Biostructures* **6,** 445–450 (2011).
57. Tripathi, T. S. & Karppinen, M. Structural Optical and Electrical Transport Properties of ALD-Fabricated CuCrO2 Films ALD - fabricated CuCrO 2 films. *Phys. Procedia* **75,** 488–494 (2016).
58. Rogé, V. *et al.* Improvement of the photocatalytic degradation property of atomic layer deposited ZnO thin films: The interplay between film properties and functional performances. *J. Mater. Chem. A* **3,** 11453–11461 (2015).
59. Liu, Y., Li, Q. & Shao, H. Optical and photoluminescent properties of Al-doped zinc oxide thin films by pulsed laser deposition. *J Alloy. Compd* **485,** (2009).
60. Lunca Popa, P., Crêpellière, J., Nukala, P., Leturcq, R. & Lenoble, D. Invisible electronics: Metastable Cu-vacancies chain defects for highly conductive p-type transparent oxide. *Appl. Mater. Today* **9,** 184–191 (2017).

61. Search, H., Journals, C., Contact, A., Iopscience, M. & Address, I. P. The activation energies of chromium , iron and nickel in gallium arsenide. **593,** (1968).
62. Karoui, F. S. & Karoui, A. A density functional theory study of the atomic structure, formation energy, and vibrational properties of nitrogen-vacancy-oxygen defects in silicon. *J. Appl. Phys.* **108,** (2010).
63. M. Needels, J.D. Joannopoulos, Y. Bar-Yam, S.T. Pantelides, and R. H. W. No Title. in *Defects in Materials* 103 (1990).
64. Biccari, F. *No Title*. *Defects And Doping In Cu2O* (2012).
65. Meljanac, D. *et al.* The influence of thermal annealing on the structural, optical and electrical properties of AZO thin films deposited by magnetron sputtering. *Surf. Coatings Technol.* **321,** 292–299 (2017).
66. Banerjee, A. N. & Chattopadhyay, K. K. Electro-optical properties of all-oxide p-CuAlO2/n-ZnO: Al transparent heterojunction thin film diode fabricated on glass substrate. *Cent. Eur. J. Phys.* **6,** 57–63 (2008).
67. Tharsika, T., Haseeb, A. S. M. A., Akbar, S. A., Mohd Sabri, M. F. & Hoong, W. Y. Enhanced ethanol gas sensing properties of SnO2-core/ZnO-shell nanostructures. *Sensors (Switzerland)* **14,** 14586–14600 (2014).
68. Wang, J., Lee, Y.-J. & Hsu, J. W. P. Sub-10 nm Copper Chromium Oxide Nanocrystals As Solution Processed P-Type Hole Transport Layer For Organic Photovoltaics. *J. Mater. Chem. C* **4,** 3607–3613 (2016).

7 Annex

7.1 Annex 1 – Annealing Conditions and Results ZnO

Table 8 – Annealing Conditions and Electrical Results for ZnO samples deposited at 200ºC

Sample (N°)	Annealing Temperature(°C)	Annealing Time(min)	Annealing Atmospher	Carrier Concentration (cm^{-3})	Mobility($cm^2/V.s$)	Rs(Ω/□)
1	300	15	N_2	$6.5 * 10^{19}$	25.9	755
2	300	30	N_2	$5.6 * 10^{19}$	26.1	892
3	450	30	N_2	$6.6 * 10^{18}$	4	$3.25 * 10^4$
4	450	15	N_2	$7.7 * 10^{18}$	2.7	$4.13 * 10^4$
5	450	15	Ar	$8.6 * 10^{18}$	6.5	$1.12 * 10^4$
6	450	30	Ar	$5.6 * 10^{18}$	3.2	$3.48 * 10^4$
7	300	30	Ar	$5.9 * 10^{19}$	21.3	494
8	300	15	Ar	$5.6 * 10^{19}$	19.4	580
9	350	15	N_2	$2.7 * 10^{19}$	18.2	1280
10	350	30	N_2	$2.3 * 10^{19}$	18	1510
11	400	15	N_2	$1.5 * 10^{19}$	8.6	5050
12	400	30	N_2	$1.1 * 10^{19}$	6.7	8830
13	450	60	N_2	$5.4 * 10^{18}$	4.2	$2.74 * 10^4$
14	450	360	N_2	$3.8 * 10^{18}$	1.8	$9.7 * 10^4$

Table 9 - Annealing plan and electrical results of ZnO samples deposited at 130º and 150ºC

Sample (N°)	Deposition Temperature (ºC)	Annealing Temperature(	Annealing Time(min)	Carrier Concentration (cm^{-3})	Mobility($cm^2/V.s$)	Rs(Ω/□)
1	130º	300	15	$2.3 * 10^{18}$	25.9	**$2.02 * 10^5$**
2	130º	300	30	$1.3 * 10^{18}$	26.1	**$4.33 * 10^5$**
3	130º	350	15	N/A	N/A	**$6.37 * 10^5$**
4	130º	400	15	N/A	N/A	**$1.01 * 10^6$**
5	130º	450	15	N/A	N/A	**$2.77 * 10^7$**
6	130º	450	30	N/A	N/A	**$3.02 * 10^7$**
7	150º	150	15	$2.6 * 10^{19}$	12.3	1750
8	150º	200	15	$3.1 * 10^{18}$	1.5	**$7.13 * 10^4$**
9	150º	250	15	$3 * 10^{18}$	2.5	**$1.11 * 10^5$**
10	150º	300	15	$2.7 * 10^{18}$	2	**$1.99 * 10^5$**
11	150º	350	15	$2.1 * 10^{18}$	1.5	**$4.17 * 10^5$**
12	150º	400	15	N/A	N/A	**$9.16 * 10^5$**
13	150º	450	15	N/A	N/A	**$5.46 * 10^6$**
14	150º	300	30	N/A	N/A	**$4.23 * 10^5$**
15	150º	300	60	N/A	N/A	**$8.04 * 10^5$**
16	150º	450	30	N/A	N/A	**$1.27 * 10^7$**

7.2 Annex 2 – Seebeck Hall Effect

The values of all the seebeck coefficients and its curves for every annealed $CuCrO_2$ samples are presented in Figure 38.

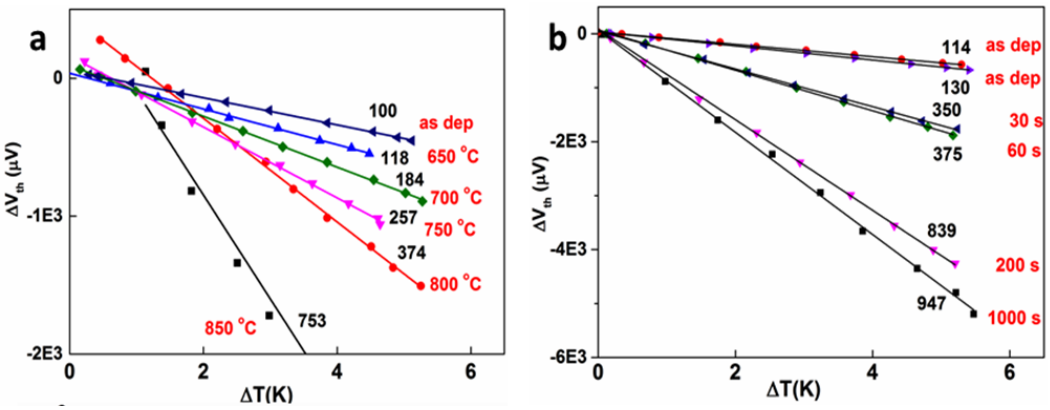

Figure 37- Seebeck measurements curve associated with $CuCrO_2$ as deposited and annealed - a) With changing temperature; b) With changing time

7.3 Annex 3 – Annealing Conditions and Results CuCrO2

Table 10 - CuCrO2 samples annealing plan and electrical results, with error extracted from Seebeck Coefficient fitting

Sample	Annealing Temperature (°C)	Time	Seebeck Coefficient ($\frac{\mu K}{V}$)	Mobility (cm^2/Vs)	Carrier Concentration (cm^{-3})	Conductivity ($\frac{S}{cm}$)
1	650	15 min	128±2	$2.4 * 10^{-2}$	$1.2 * 10^{21} \pm 2.7 * 10^{19}$	4.81
2	700	15 min	184±2	$1 * 10^{-3}$	$6.6 * 10^{20} \pm 1.5 * 10^{19}$	0.108
3	750	15 min	257±3	$1.2 * 10^{-4}$	$2.9 * 10^{20} \pm 9.9 * 10^{18}$	$5.63 * 10^{-3}$
4	800	15 min	374±4	$1.3 * 10^{-4}$	$7.3 * 10^{19} \pm 3.5 * 10^{18}$	$1.49 * 10^{-3}$
5	850	15 min	753±25	$3.5 * 10^{-3}$	$9.3 * 10^{17} \pm 2.7 * 10^{17}$	$5.21 * 10^{-4}$
6	900	30 s	340±2	$1.1 * 10^{-3}$	$1.1 * 10^{20} \pm 2.6 * 10^{18}$	0.02
7	900	60 s	360±4	$9.9 * 10^{-4}$	$8.9 * 10^{19} \pm 4 * 10^{18}$	0.014
8	900	200 s	850±9	$3.7 * 10^{-2}$	$3 * 10^{17} \pm 3 * 10^{16}$	$1.8 * 10^{-3}$
9	900	1000 s	947±13	$1.4 * 10^{-2}$	$9.4 * 10^{16} \pm 1.5 * 10^{16}$	$2.03 * 10^{-4}$
10	900	4000 s	N/A	NA	NA	NA

The Seebeck coefficient error was extracted from the fitting and the Carrier Concentration error was calculated using equation 12

$$\frac{\delta p(S)}{\delta S} * \Delta S \text{ (equation 12)}$$

7.4 Annex 4 - Software

The junction is always designed with a P-type on the left side with 100 nm and on the right side the ZnO n-type also with 100 nm. On both sides, it is considered to have a perfect contact. Firstly, it was tested with several different carrier concentrations where it is important to have a well-defined depletion region and an off-state without any bias.

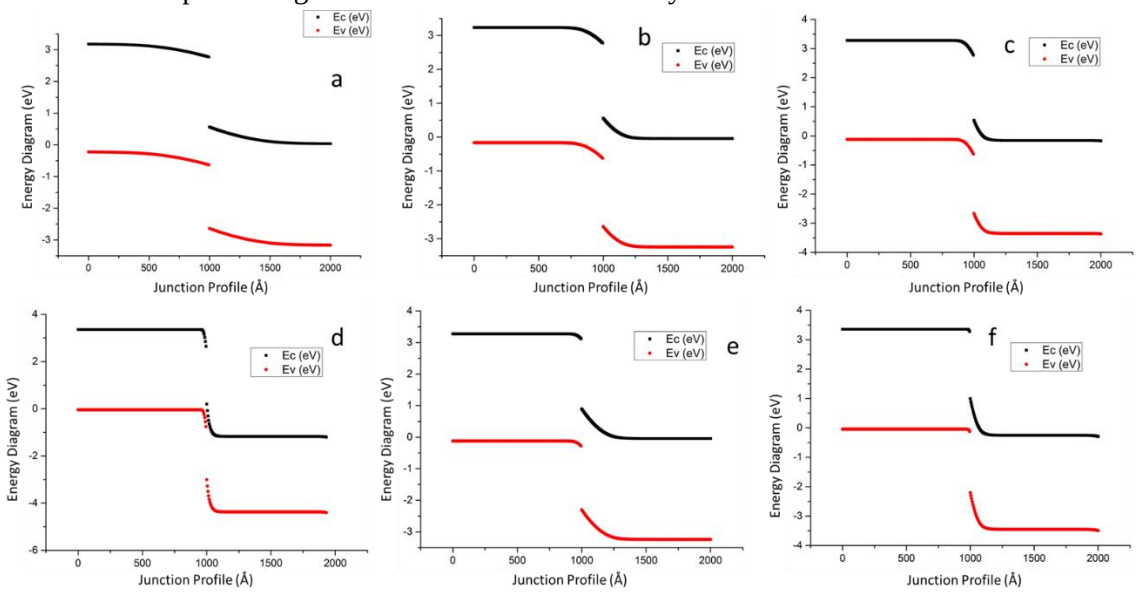

Figure 38 - Simulated junctions with same carrier concentration on P and N side where is represented the energy levels projection as function of the junction length - a) Carrier concentration $10^{17}cm^{-3}$, b) Carrier concentration $10^{18}cm^{-3}$, c) Carrier concentration $5 * 10^{18}cm^{-3}$, d) Carrier concentration $10^{20}cm^{-3}$, e) Carrier concentration on p-side $5 * 10^{18}cm^{-3}$ and n-side $10^{18}cm^{-3}$, f) Carrier concentration on p-side $10^{20}cm^{-3}$ and n-side $10^{19}cm^{-3}$

From this simulation, it is possible to see that there are various possible solutions that could work, having a good type-II band alignment and with an OFF-state with 0 bias. Solutions such as the represented in Figure 39 – a), Figure 39 – d) Figure 39 – f) would not be the best candidates for having a potential ON-state with 0 bias in the first case, and a very small depletion region in the last cases what could induce tunnelling effects. Hetero-carrier concentration junctions can be a possibility provided that the more doped region is in the P-side, such as Figure 39-e), but still in the limits of a maximum carrier concentration expected up to $10^{19}\mathrm{cm}^{-3}$.

The simulation could be used for further studies of C-V curves but unfortunately it was not possible to extract the relative dielectric constant that would allow this feature.

7.5 Annex 5 – Junction Optical Images

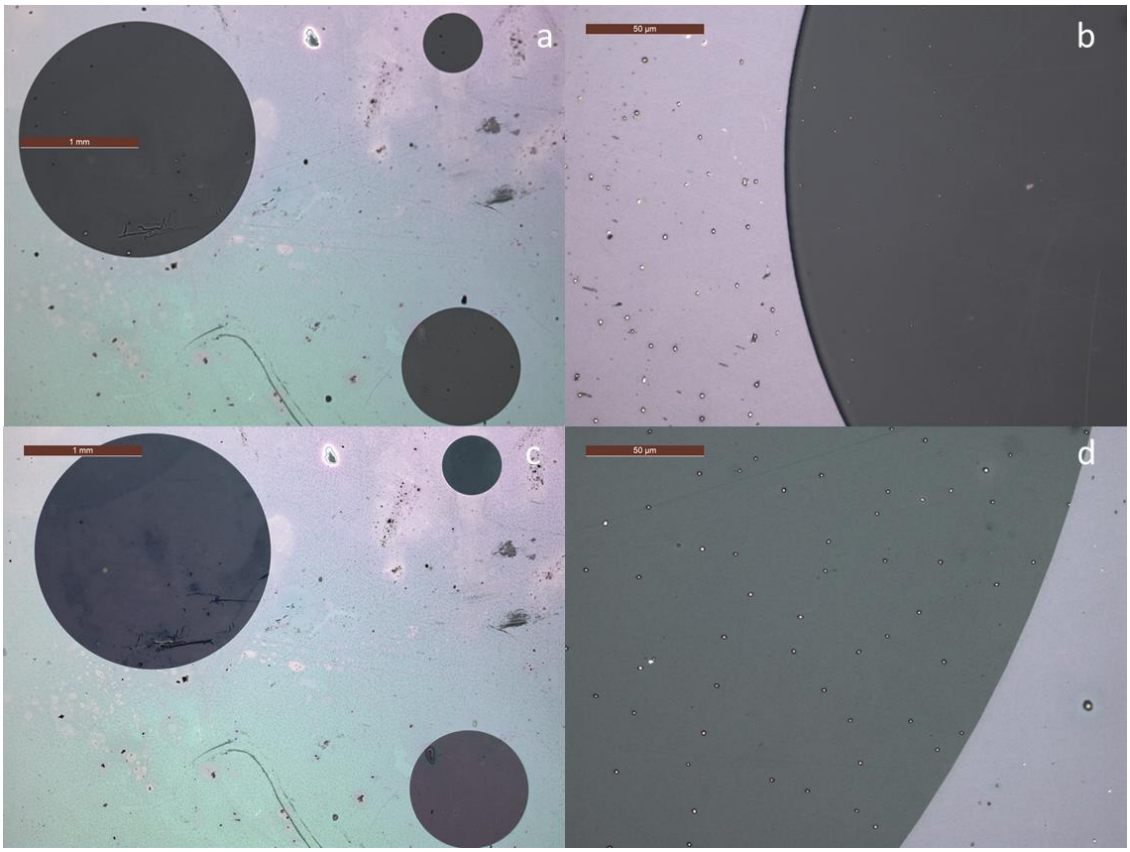

Figure 39 - Junction Optical Images of the junction in sample 2 before – a, b and after the removal of the photoresist – c, d

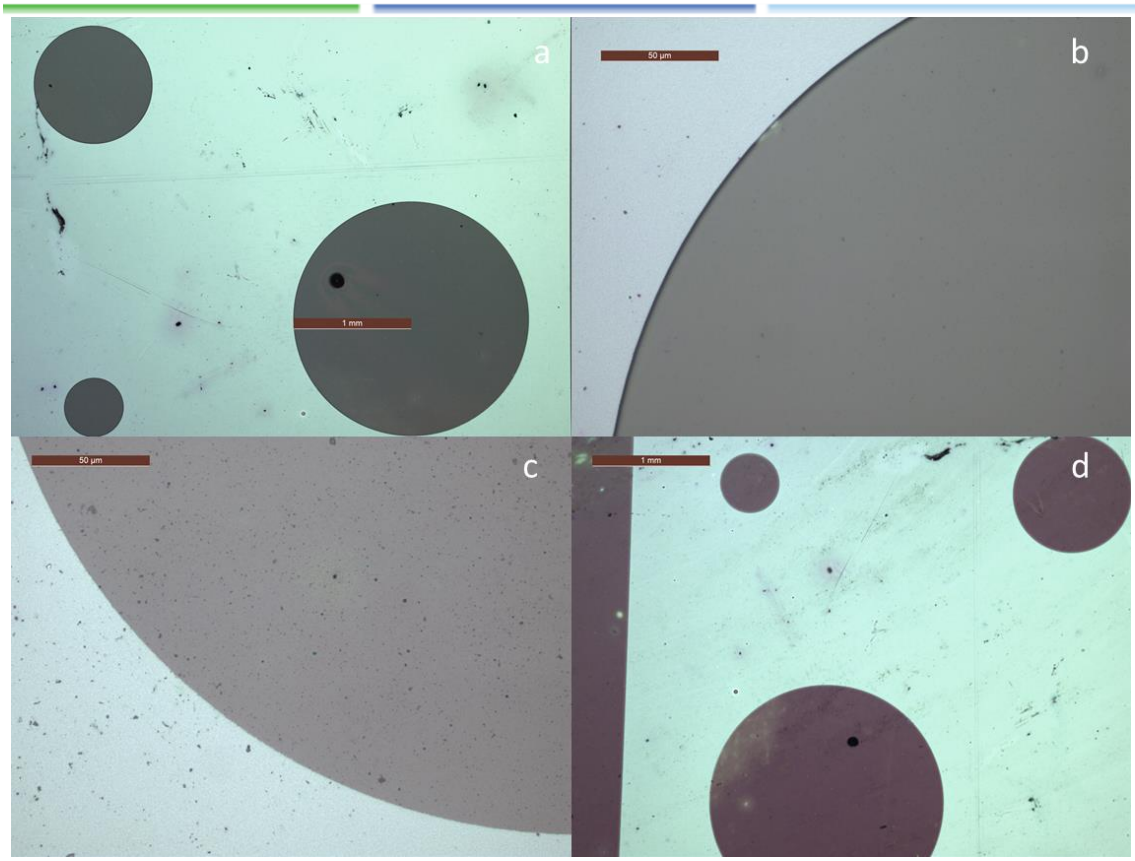

Figure 40 - Junction Optical Images of the junction in sample 1 before – a, b and after the removal of the photoresist – c, d

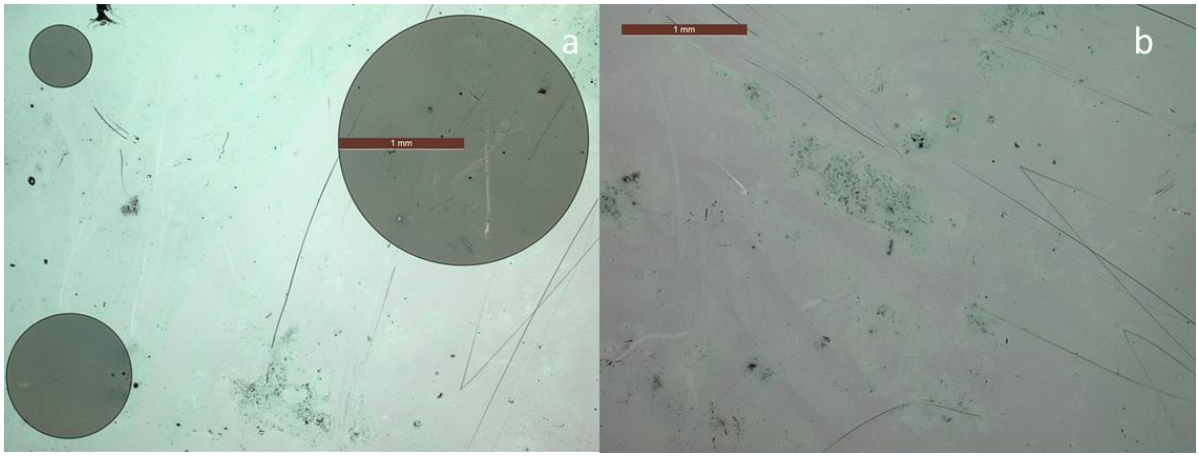

Figure 41 - Junction Optical Images of the junction in sample 3 before – a and after the removal of the photoresist – b, showing the removal of all the patterned layers